Analysis of fatigue failure of bone using stress – strain curve for improved prosthesis designing

A Major Project dissertation submitted

In partial fulfilment of the requirement for the degree of

Master of Technology

In

Biomedical Engineering

Submitted by

Matiul haq ansari

(DTU/13/M.TECH/391)
Delhi Technological University, Delhi, India

Under the supervision of

Dr. Jai Gopal

Department of Biotechnology
Delhi Technological University
(Formerly Delhi College of Engineering)
Shahbad Daulatpur, Main Bawana Road,
Delhi-110042, INDIA

DECLARATION

I Matiul haq ansari hereby declare that this submission is my own work and that, to the best of my knowledge and belief, it contains no material previously published or written by another neither person nor material which to a substantial extent has been accepted for the award of any other degree or diploma of the university or other institute of higher learning except where do acknowledgement and references has made in the text.

Signature:

Matiul haq ansari

(DTU/13/M.TECH./391)

ACKNOWLEDGEMENT

I take this opportunity to express my deepest gratitude and appreciation to all those who have helped me directly or indirectly towards the successful completion of my major project- II.
I express my sincere thanks and deepest gratitude to my guide Dr. Jai Gopal sir Department of Biotechnology, DTU for giving his, sagacious guidance, advice and supervision throughout my project work. I am highly impressed to his intelligence well organized and enthusiastic approach towards goal oriented research. I am privileged to have been his student. I am greatly thankful to him for providing excellent laboratory facilities, perfect scientific environment as well as opportunities to explore scientific world.

I am greatly thankful to all respected faculties of the Department of Biotechnology, DTU for their efficient teaching, generous support and providing me clear concept for research.
I am thankful to my friends and family for throughout provoking discussion and making stay very pleasant.

Matiul haq ansari

DTU/13/M.TECH./391

CONTENTS

LIST OF TABLES

LIST OF GRAPH

LIST OF FIGURES

ABSTRACT

Mathematical studies of mechanical and rheological behavior of synovial fluid closely or directly connected with human physiology play an important role in several areas of Biomedical Engineering. The fundamental research on biological systems plays an important role for the future medical treatments or bio-engineering development. In this thesis, the application of weibull statistics for load cycle analysis of fatigue failure of bone has been studied. It was found that the synovial fluid reacts very sensitively to the magnitude of shear stress and fatigue occur on the articulating surface of the knee joint during knee motions namely flexion and extension and vice versa. An S-N curve for knee joint was developed in order to study the variation of failure stress with respect to number of load cycle. A reliability study of bone failure was carried out for a wide variation of stress cycles and also for different weights. As probability of failure increases with aging, such studies were carried out to determine fracture strength of bone in different ages and with different weights.

INTRODUCTION

1.1 Brief Overview

Bone is considered as optimally an anisotropic material that is able to bear stress load of different mechanical properties in different directions. There is no specific strength which represents their mechanical behaviour. There is a need of statistical approach for evaluating the strength of bone.

In this thesis, by using realistic Weibull shape and scale parameter for the problem concern which deals with the fatigue failure of articular surface of the human knee joint, the flow velocities of synovial fluids in the human knee joint can be simulated.

The intention behind thesis work is not to stipulate answers to the unanswered questions, but try to deal with the problems from a different charactors. This comprises effort to explain the combinatorial nature of fatigue failure in bone; that may help to fetch basic idea of engineering layout contrary fatigue failure through S-N curve. S-N curve shows the graphical representation of stress amplitude versus the number of stress cycles before the fatigue failure. Fatigue failure occurs in Synovial joint primarily due to rheological behaviour and effect related to the flow of Synovial Fluid between the opposite Surface of Articular Cartilage.

Using weibull distribution, the reliability of bone in terms of its fracture strength was presented in graph. Weibull distribution was used as a practical approach to determine reliability values of stress produced by a flow of synovial fluid during knee rotational motion.

1.2 Purpose of study

Bones are often subjected to cross flow vibration when Synovial fluid flows over the different contours of articular surfaces. Significantly cross flow vibration will occur when the natural vibrational frequency of bone matches with the frequency of periodic vortex shedding of the concerned synovial fluid. Significant periodic vortex shedding leads to fatigue failure of bone for which study of S-N curve is very much necessary. To study the fatigue failure of bone due to induced stress by flow of synovial fluid. In the scope of work, S-N curve has been generated in case of bone fatigue by weibull statistics.

Fracture Strength has been statistical analyzed by the Weibull Distribution method. Weibull Reliability Distribution describes the fracture strength of Articular Surface of the synovial joint. The probability of the failure can also be determined by the weibull distribution at high stress value.

1.3 LITRATURE REVIEW

The frequency of the synovial fluid determines by the principle formula of the vortex shedding will be matched with the natural frequency of the bone under design condition to get the S-N curve. Using weibull distribution, find the reliability of bone in terms of its fracture strength.

X. Fan et al. [2] study on the weibull modulus, k, versus volume distinct porosity, P. Porous brittle material are commonly used as filters, catalyst supports for reactions , solid oxide for fuel cells and biomedical materials. In this study, analyze a combined data set collected from the literature that represents work from 17 different research groups, 8 different materials and more than 1560 oxide and non-oxide specimens, the k versus P plot is "U-shaped", k values for $P< 0.1$(Region I) and $P>0.55$(Region III), and narrow band of k values in the intermediate porosity region of $0.1<P<0.55$(Region II). Part II of this study focuses on the p dependence of the mean fracture strength and the Young's modulus for HA specimens tested in Part I along with given literature data for other brittle materials.

Michael et al. [3] paper analyzes micro tensile tests on unfilled resins and adhesive bonds between restorative resin composite and dentine in terms of reliability using the Weibull probability of failure method. Weibull analysis provides a method for determine the reliability of strength measurements in the analysis of given data from bond strength and tensile tests performed on dental restorative materials.

Martin et al. [4] study of the fatigue life of cortical bone screws under conditions which simulated in vivo usage was performed. They found that the two most important factors that influencing fatigue life of respective was axial screw tension (the force normal of the plate to bone) and the cyclic shearing loading. They found that data from the fatigue experiments revealed the classical fatigue relationship that increased loads led to a shortened fatigue life. The statistical analysis of the data indicated that load is the primary determinant of the life of the screw.

Petcharatana et al. [5] study the rheological characterization of synovial fluid form 22 patients which undergoing total knee arthroplasty and three commercially available viscous supplements is performed. Synovial fluid in osteoarthritis (OA) patients exhibits non- Newtonian shear thinning behaviour and viscoelastic properties. The high – molecular-weight viscosupplements have greater viscoelasticity that of low molecular-weight viscosupplements.

R.Blickhan et al. [6] in this paper, the ranges of physiological possible hopping frequencies, a human hopper selects a frequency where the largest amount of energy can be delivered and still be stored elastically. During running and hopping animals use flats angles of the landing velocity resulting in maximum contact length of distance. In this situation, the reaction force from ground is proportional to total specific contact time and, total displacement is proportional to specific contact time and also proportional to the square of the step duration. Contact time and hopping frequency cannot simply determine by the natural frequency of the spring-mass systems, but are influenced largely by the vector of the landing velocity.

M.Husriu Dirikolu et al. [7] study on the fracture strength of a carbon-epoxy composite plate has been statistically analyzed by weibull distribution. By using weibull distribution method, we can find the probability distribution according to which the material will fail was obtained. In this respect, the weibull distribution allows researchers to describe the fracture strength of a composite material in terms of a reliability function.

R.J.Morrissey et al. [8] determine the effects of test frequency on the high cycle fatigue (HCF) behavior of Ti-6Al-4V. In this frequency dependence that varies with stress ratio (R). At low R, the fatigue strength increases with increase in frequency. As R is increased, this trend continues until a transition zone is achieved. Above this transition the frequency effects seem to vanish at the lower frequency, but it is still apparent at higher frequency. The ductile behavior is characterized by void nucleation and growth and the apparent lack of the fatigue crack initiation and growth that is evident at low stress ratios.

S.H Teoh et al. [9] study on the fatigue–wear corrosion and environmental stress cracking are common. It is not possible to avoid failure but has to be focused on predictive tools to enable more accurate prediction as to avoid catastrophic failure in vivo. This paper presents an overview of fatigue fracture problems arises in metallic, polymeric and ceramic implant materials, looks at some recent techniques of testing and discusses the future developments of fracture and wear resistant biomaterials.

Gregory M. Williams et al. [10] consider the roles of shape, loading behavior and motion in synovial joint mechanobiology and their incorporation into the designs, fabrication, and testing of engineered partial or whole joints. Also various incidences like degeneration, degree of impairment and efficacy of some current treatments may be considered as critical factors in choosing a target for joint bioengineering. The form and function of native joint may guide the design of engineered joint- scale constructs with respect to shape, size and maturity. Fabrication challenges for the joint scale engineering include controlling chemo-mechano-biological microenvironment that help to promote the development and growth of multiple tissues with integrated or lubricated surfaces into anatomical shapes and

developing joint-scale bioreactors which nurture and simulate the tissue with loading behavior and motion, finally, evaluation of load –bearing and tribological properties can be range from tissue to joint scale and can focus on biological structured at present or after adaptation.

Mirza Biscevic et al. [11] study to the mathematically approximate the shape of the femoral articulating cartilage line and compare radiuses of condylar curves within and between males and females. Radiuses of medial and lateral condylar curves were calculated from the side view knee X-ray by original mathematical equation. Males had longer curve radiuses of both condoyles. Approximation of the radiuses of femoral condoyle curves is a useful method in anthropometric, radiological and virtual calculation of the knee geometry and other ellipsoidal structures in our body, like wrist, scull segments, dental arches, etc.

1.4 Key objectives

The above discussion will render the following conclusion which will help to decide key objectives:

- To obtain the Fatigue Failure at the surface of articular cartilage of the synovial joint due to the cross vibration flow of synovial fluid by using the curve between stress amplitude and load cycles (S-N curve).
- To determine the fracture strength in terms of reliability function by using Weibull distribution.

Hence, key objectives of this research are as below:

- Theoretical estimation of natural frequency of knee joint by using spring-mass model to avoid possible fatigue failure.
- Theoretical estimation of the critical velocity of synovial fluid flowing in joints by matching the frequency of periodic vortex shedding with the natural frequency of knee joint.
- To determine the number of stress cycles by using the expected number of hours per year in critical velocity range.
- To determine the reliability function by using Weibull Distribution.

2.1 Bone Mechanics:

Bone is a structural support of the human body. Bones forms the building blocks of the skeletal system which protects the internal organs, provides kinematic links, provides muscle attachment sites, and facilitates muscle actions and body movements. Bone matrix has unique structural and mechanical stress bearing properties that

allow it to carry out these functions. Bone is unique; it is capable to self repairing of its own injured tissue. Bone is an anisotropic in nature. Due to this, it alters its shape, mechanical behaviour and mechanical properties according to changes in mechanical demand of the body. The major factor that influence the mechanical behaviour of bone is depends on the composition of bone, the mechanical properties of the tissues comprising the bone, the size and geometrical structure of bone, and the direction, magnitude and the rate of applied loads on bones.

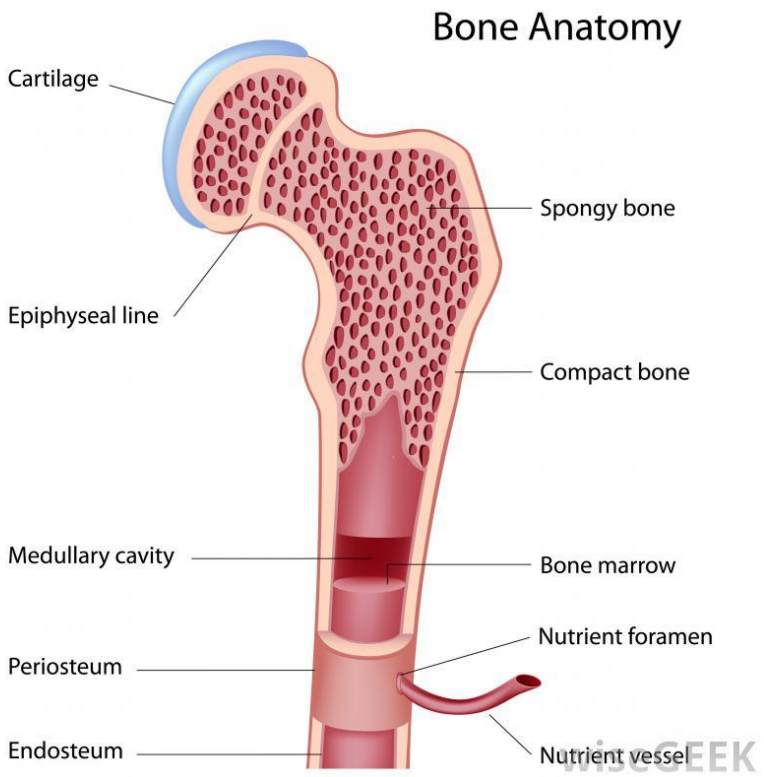

Fig. 3.1 Schematic presentation of bone anatomy

There is a connective tissue in bone that has the potential to repair bone and regenerate. It is a composite of mineral matrix and collagen fibres. In this a rigid matrix of calcium salts around the protein fibres. Rigidity gets from minerals elasticity and strength gets from proteins. Bone is a hard connective tissue and forms rigid skeleton. Its yield strain is small (less than .01) and elastic modulus is high (18GPa) as compared with normal walking stress. Stress strain relation is linear in elastic range. Bone is frequently considered as a linear elastic material. Bone has organized in microstructure i.e. lamellar (layered), Harversian (tubular) and trabecular (spongy, fabric-like).

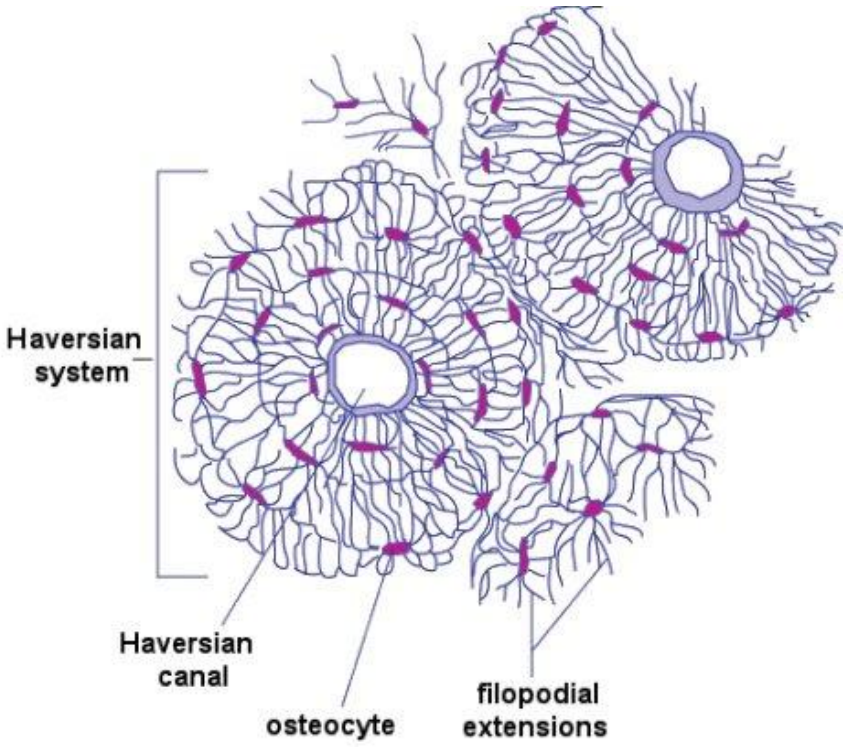

Fig.3.2 Schematic diagram of cross section of bone showing haversian canal system

Bone has different shapes such as long bones, short bones, flat bones and irregular bones. Long bones are cylindrical and hollow in nature to achieve strength and minimize weight.

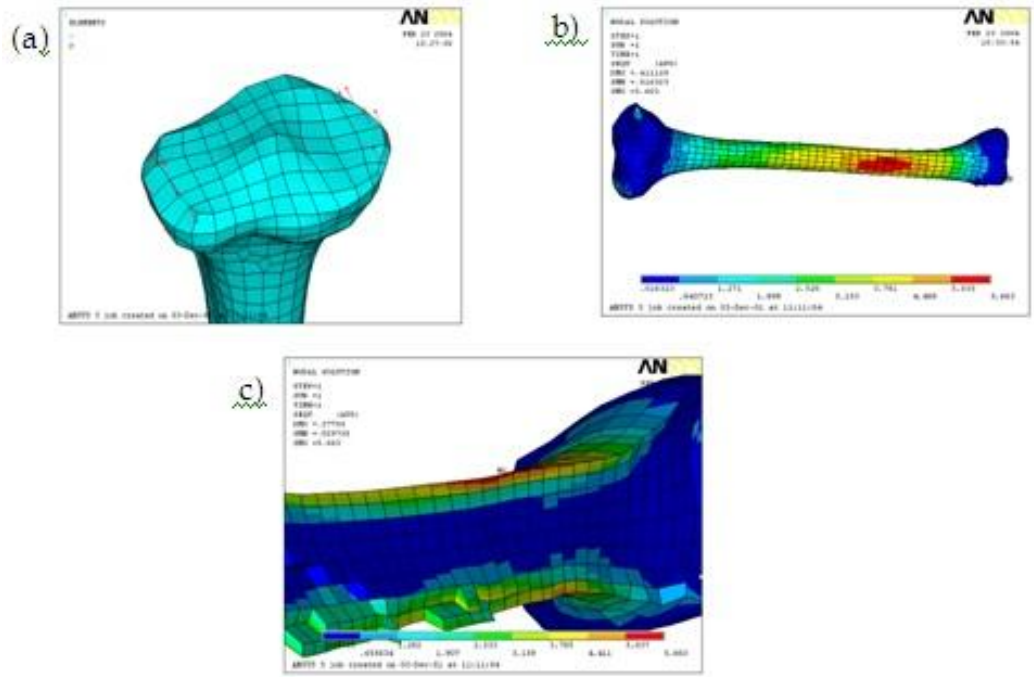

Fig.3.3 model of tibia bone showing stress regions

The stress-strain behaviour of bone is also contingent on the orientation of bone with respect to the direction of loading. This anisotropic material behaviour is shown in Figure 2.1. Indicating that the cortical bone specimens loaded in the transverse direction fail in a more brittle manner than in the longitudinal direction.

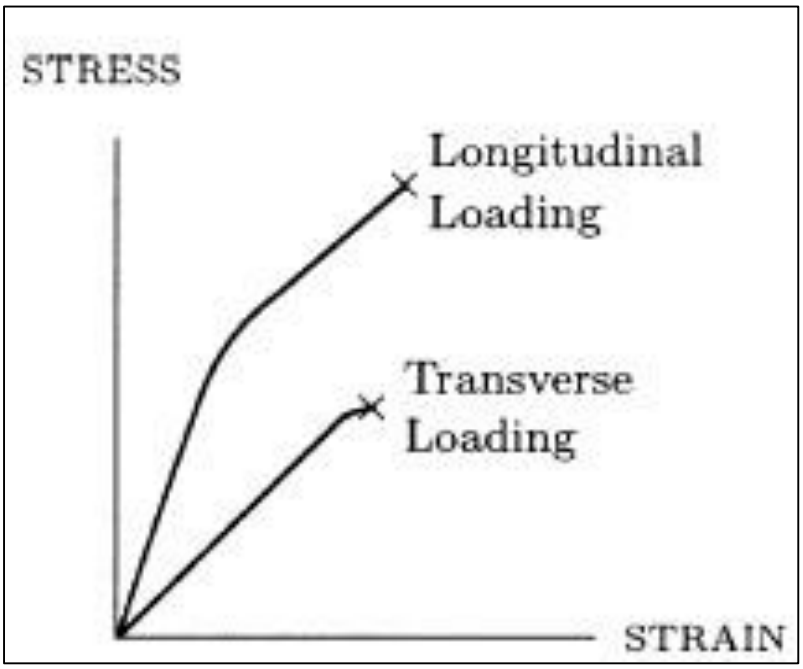

Fig. 2.1: The direction-dependent stress–strain curves for bone tissue [11].

Reilly and Burstein [27] analyzed the mechanical properties of the diaphyseal bone of femur under various modes of loading, as shown in Table 2.2 [27] indicating that the values of Ultimate strength and elastic modulus of cortical bone is higher in the longitudinal direction rather than in transverse direction that means cortical bone is more stronger and stiffer in the longitudinal direction than in the transverse direction.

Loading Mode	Properties	Femoral cortical bone
	ELongitudinal (GPa)	17
	ETranverse (GPa)	11.5
	ρ Density (gm cm^{-3})	3.3
Longitudinal		
	Ultimate Compressive Strength (MPa)	193
	Ultimate Tensile Strength (MPa)	133
	Ultimate Shear Strength (MPa)	68
Transverse		
	Ultimate Tensile Strength (MPa)	51
	Ultimate Compressive Strength (MPa)	133

Table 1.1: Mechanical properties of typical cortical bone by Reilly et al [27](1 GPa = 10^9 Pa, 1 MPa = 10^6 Pa)

Lotz et al. [29] analyzed the anisotropic mechanical properties of the metaphyseal bone. Table 1.2 showing properties of the metaphyseal bone reported by Lotz et al. which can compare with properties of the diaphyseal bone reported by Reilly et al, indicates major differences.

Properties	Metaphyseal cortical shell
ELongitudinal (MPa)	9650
ETranverse (MPa)	5470
ρ Density (gm cm^{-3})	1.62

Table 1.2: Mechanical properties of the metaphyseal bone Lotz et al. [29].

Load characteristics of a bone include:

- Direction of the applied force
- Tension
- Compression
- Bending
- Torsion

- Shear
- Magnitude of the load
- Rate of load application

Main functions of bone are:-

- Mechanical support
- Haematopoiesis (Formation of blood cellular components)
- Protection of vital structures
- Mineral homeostasis

2.2 Analysis of Knee joint

The knee joint is located between the body's two longest lower arms which makes it the most complicated and most incongruent joint in human body. It sustains high forces and susceptible to the chronic diseases and injuries.

In knee joint, there are three bones:

- The femur (the thigh bone)
- The tibia (the shin bone)
- The patella (the knee cap)

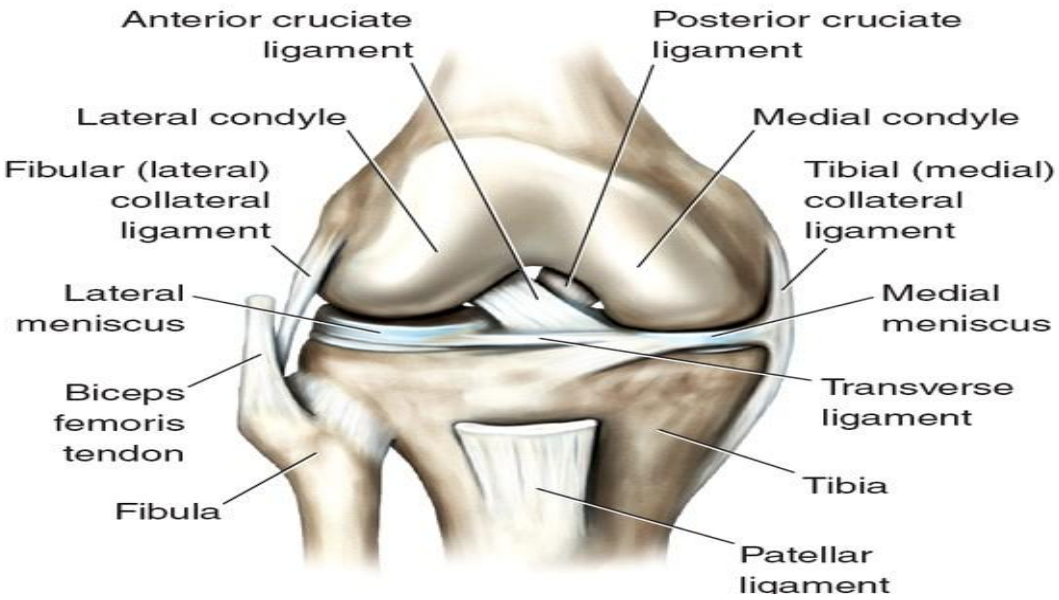

Fig.3.4: The human knee joint [1]

In knee joint there are also two ligaments on either side of the knee, called as the medial and lateral collateral ligaments, which stabilize the knee from side by side. In the centre of knee joint there is a ligament in the form cross that stabilizes the knee from front to back during normal and athletic activities. The main function of

the ligament is to make sure that load transmitted through the knee joint is centred within the joint to minimize the amount of wear and tear process of the cartilage inside the knee joints.

The peripheral surfaces of the knees are covered with a layer of cartilage. There are two shock absorbers on either side of the knee joint. These two structures are called the medial meniscus and lateral meniscus.

2.2.1. Meniscus

It is horse shoe shaped shock absorbers that help to both centre the knee joint during physical activity and try to minimize the amount of stress on the articular cartilage.

In knee, the menisci and the surface cartilage both produces frictionless gliding surface. The knee is an incredible joint. It is strong, flexible and very tough. The main muscles that help to move the knee joint are the quadriceps and hamstring muscles. The quadriceps that attaches to the patella via the quadriceps tendon, the patella is attached to the tibia bone via the patellar ligament knee extends when the quadriceps muscles contact and knee flexes when the hamstring muscles contract.

Averages radiuses of condoyler curves were between 4.5cm & 1.7cm medially and between 3.2cm &1.8cm laterally for 0 degree and 90 degree flexion contacts respectively. For intercondyler width was 2.20cm $\pm$0.18cm [11]. It varies person to person.

Average diameter of both (medially and laterally) =11.2cm
Average diameter of intercondyler = 2.20cm

Human joints are specifically for transmitting large normal loads from one bone to another while allowing an efficient relative's motion in a directional tangential to the surfaces. Loads vary considerably from joint to joint and from moment to moment and so it is intended to look at specific joint and activate to establish the patient features [12].

In normal walking, the sliding velocity in the knee varies with time. During walking, sliding velocity is low at high load and sliding velocity is high at low load.

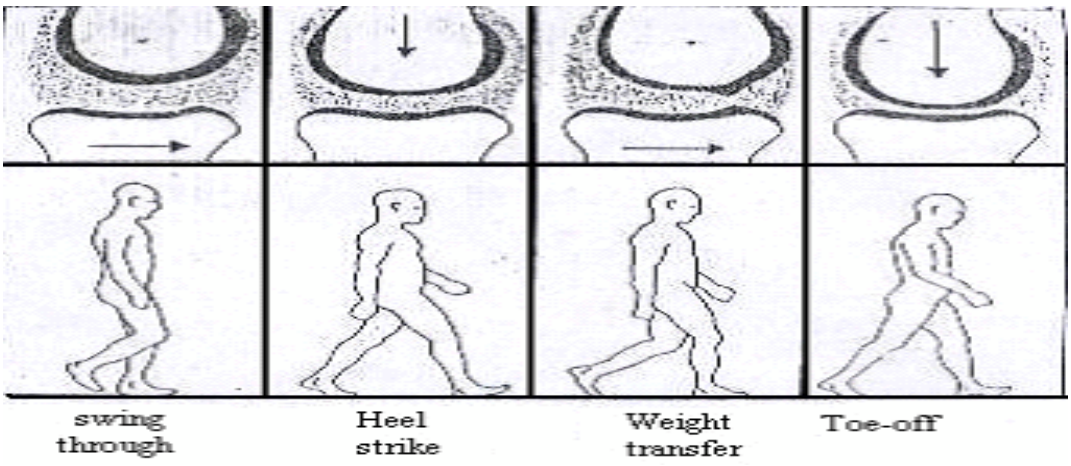

Fig.3.5: Lubrication mechanism of right knee joint [12].

At 'swing phase', where a small load coincides with a high sliding velocity. In this foot has left the ground and leg is swing freely, a thick film of synovial fluid can be entrained into the space between the cartilage. When heel strikes to the ground, the entraining velocity is reduced towards zero. Here, the thick film generated begins to squeeze out and the film thickness reduces. Load is applied for short time in normal walking; the film mechanism is able to maintain a viable film of lubricant during this stage. As the cycle progresses, the load of the knee decreases and the entraining velocity increases.

This phase of the walking cycle suggest elasto hydrodynamic lubrication. Finally at the 'Toe off' position, load is maximum and the entraining velocity is very low and "squeeze film" lubrication can help to maintain a fluid film and prevent surface to surface contact.

Spring mass model of human body have been developed to study the response of the body reaction with the ground during running and hopping**.**

General principles of vibration theory relate the stiffness and mass of a structure (knee joint) to its natural frequency. Spring mass model of the human knee joint is expressed as following

2.3 Analysis of Ankle joint

The ankle joint is a complex mechanism. The ankle is actually composed up of two joints: the subtalar joint and another true ankle joint. Where true ankle joint is composed of three bones, the tibia bone which forms the inside, or medial, portion of the ankle joint; the fibula bone which forms the lateral or outside portion of the ankle; and the talus bone underneath. The true ankle joint is mainly responsible for the up-and-down motion of the foot.

Apart from the true ankle joint is the second part of the ankle, the subtalar joint, which consists of talus bone on top position and calcaneus bone on the bottom. The subtalar joint are allows side-to-side motion of the foot up to some extent.

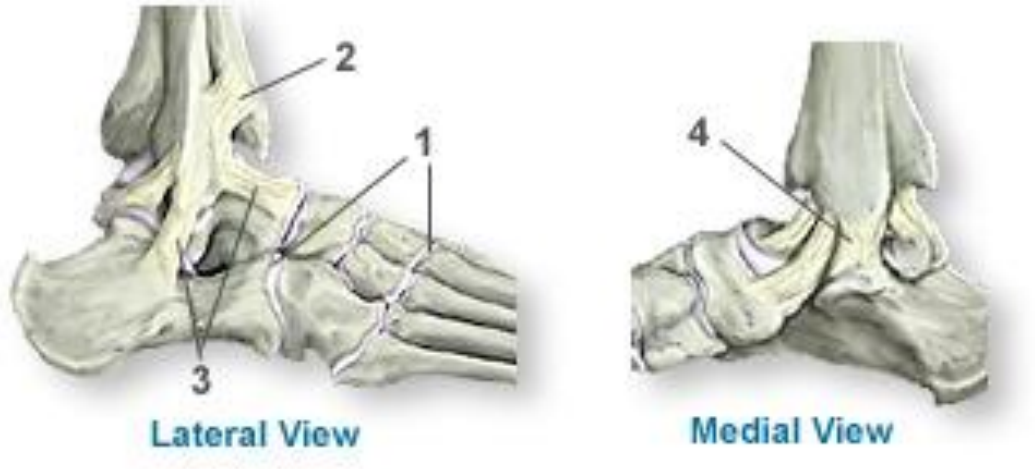

Figure 3.6: Photographs of an ankle joints showing the individual bones and joints.

The ends of these bones in the ankle joints are covered by articular cartilage (1). The major ligament parts of the ankle are: the anterior tibio-fibular ligament (2), which connects firmly the tibia to the fibula bone; the lateral collateral ligaments (3), which attaches the fibula bone to the calcaneus bone and gives the ankle joint to lateral stability; and, on the medial side of the ankle joint, the deltoid ligaments (4), which connects the tibia bone to the talus bone and calcaneus bone and provide medial stability.

These components of ankle joint, along with the muscles and tendons of lower leg, work together to manage the stress ankle joints endures as we walk, run, and jump.
The ankle joint is also classified as a diarthrodial or synovial joint. Diarthrodial joint contains semi liquid, synovial fluid. Between the ankles joint, the synovial cavity is present that contains synovial fluid for lubrication mechanism, shock absorbing & joint nourishment mechanism processes, which is surrounded by articular capsule which help to integrate the two articulating bones at joints. The ankle joints are also covered by hyaline (articular) cartilages whose main function is to absorb shock & reduce friction during movement of bones. Several ligaments in joints connect the ankle bones together to further stabilize the joint. Muscles and tendons of joints provide actuation forces that permit limited range of motion during walk jump and run.

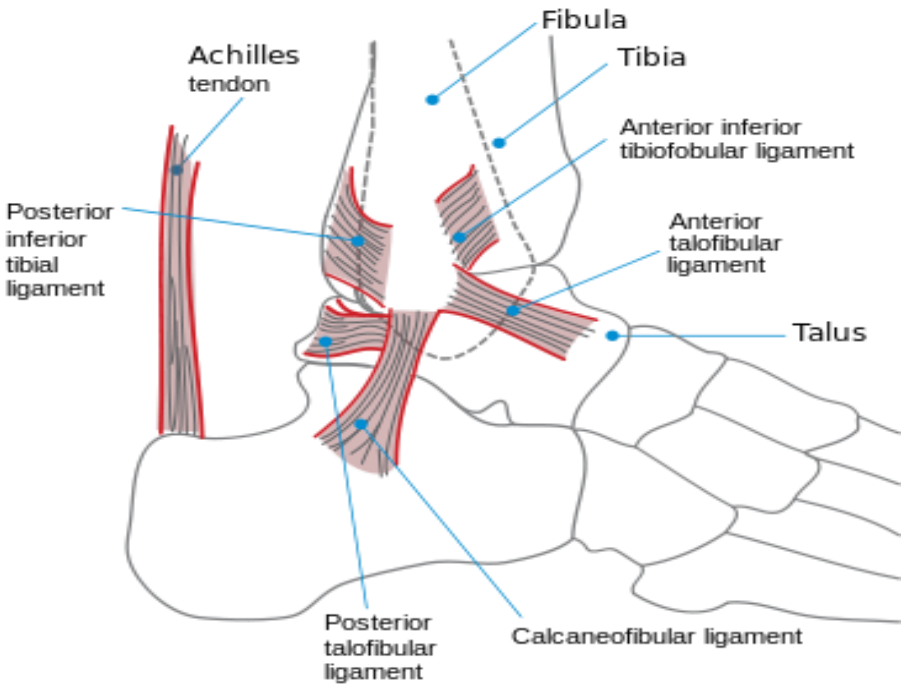

Fig.3.7: Photograph of ankle joint showing the tendons and ligaments.

2.4 Tibia

The tibia is a large bone located along with fibula bone in the lower leg of the human body. The tibia bone is also known as the shin bone or the shank bone. The tibia bone is positioned in the lower front portion of the leg of the human body. It is the bigger bone of the two bones in the shin area. The other bone in that region is known as the fibula bone. These two bones are collectively connecting the ankle bone to the knee in the human body. These bones are located in between the ankle and the knee of the lower leg in the human body. The tibia bone is located in the medial side of the lower leg. This bone is directed vertically in the leg of the human body. The tibia is a type of long bone in the lower leg and is the second largest bone in the human body. The tibia is also often referred to as the strongest weight bearing bone in the human body. The tibia bone carries all the body weight of a human being.

The tibia bone is categorized as a long bone and is as such composed of a diaphysis and two epiphyses region. The diaphysis region is the midsection of the tibia bone also known as shaft or body. While the epiphyses region are the two rounded extremities of the bone; an upper part (also known as superior or proximal) closest to the thigh and a lower part (also known as inferior or distal) closest to the foot. The tibia bone is most contracted in the lower third and the distal extremity is smaller than the proximal.

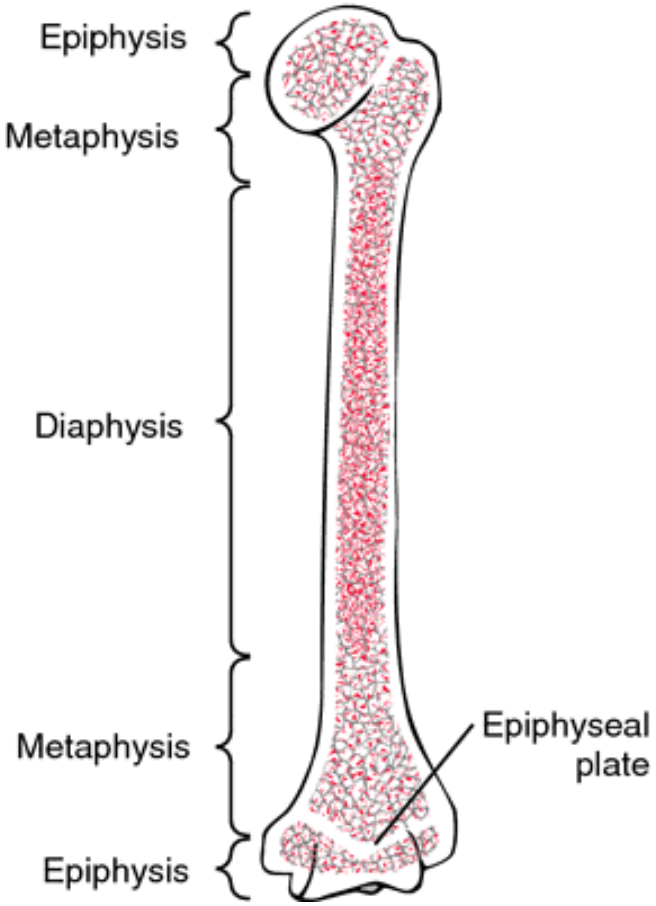

Fig.3.8: Tibia bone showing different regions

The proximal or upper extremity of the tibia bone is expanded in the transverse plane with a medial and lateral condoyle, which are both flattened in the horizontal plane of surface. The medial condoyle part is the larger of the two and is better supported over the shaft bone. The upper surfaces of the condoyle part articulates with the femur bone to form the tibio-femoral bone joint, the weight bearing part of the knee joint.

The medial and lateral condoyles of joint are separated by the intercondoylar area, where the cruciate ligaments and the menisci attach. In this region, the medial and lateral intercondylar tubercle forms the intercondylar eminence. Together with the medial and lateral condoyle part, the intercondylar region forms the tibial plateau, which both articulates with and is anchored to the lower extremity of the femur bone. The intercondylar eminence region divides the intercondylar area into an anterior and posterior part. The anterolateral joint regions of the anterior intercondoylar area are perforated by numerous small openings for nutrient channels. The articular surfaces of both condoyles are concave nature, particularly central part. The flatter outer margins of the bone are in contact with the menisci. The medial condoyles superior surface is oval in shape and extends laterally onto the side of medial intercondylar tubercle region. The lateral condoyle's superior surface is more circular in shape and its medial edge extends onto the side of lateral intercondylar tubercle.

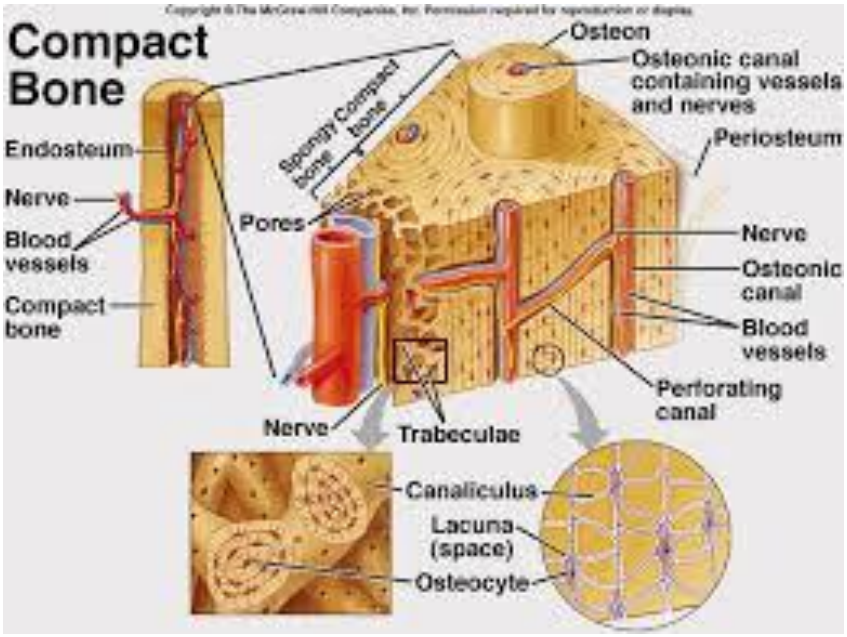

Fig.3.9: Schematic cross section of bone showing different parts of bone

The posterior surface of the medial condoyle bone bears a horizontal groove for part of the attachment of the semi membranous muscle structure, whereas the lateral condoyle bone has a circular facet for articulation with the head of fibula bone. Beneath the condoyle, the tibial tuberoses which serves for attachment of the patellar ligament, a continuation of the quadriceps femurs muscle.

The shaft or body of the tibia bone is triangulate in cross-section area and forms three borders: An anterior border, medial and lateral or interosseous border. There are three borders forms three surface; the medial, lateral and posterior. The forward flat part of the tibia bone is called the tibial condoyles, often confused with the fibula. The lower extremity of the tibia is much smaller than the upper extremity and presents five surfaces; it is prolonged downward on its medial side as a strong process, the medial malleolus. The region of lower extremity of the tibia bone together with the fibula and talus forms the ankle joint.

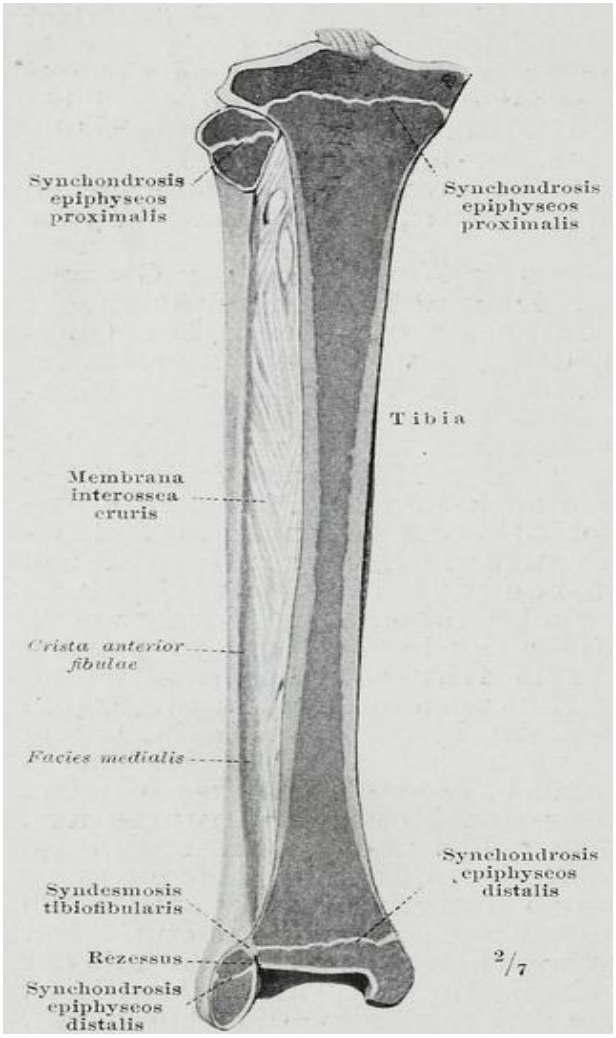

Fig.3.10: Photograph of a tibia- fibula bone showing synchondrosis epiphyscossis region.

2.4.1 Tibia joints

The tibia bone is a part of four joints; the knee, ankle, superior and inferior tibio-fibular joint. In the knee joint, the tibia forms one of the two articulations with the femur bone, often referred to as the tibio-femoral components of the knee joint. This is the weight bearing part of the knee joint. The tibio-fibular joints are the articulations between the tibia and fibula bone which allows very little movement. The proximal tibio-fibular joint is a small plane joint in the knee region. The joint is formed between the under surface of the lateral tibial condoyle bone and the head of fibula bone. The joint capsule is reinforced by anterior and posterior ligament of the head of the fibula bone. The distal tibio-fibular joint (tibio-fibular syndesmosis) is formed by the rough surface, the convex surface of the medial side of the distal end of the fibula bone, and a rough concave surface on the lateral side of the tibia bone. The part of the ankle joint known as the talocrural joint, is a type of synovial hinge joint that primarily connects the distal ends of the tibia and fibula bone in the lower limb

with the proximal end of the talus bone. The articulation between the tibia bone and the talus bone bears more weight than between the smaller fibula and the talus bone.

The bones of the lower extremity, i.e., tibia bone may be considered as having two main functions: (I) as a supporting structure which transfers body weight from knee joint to the ankle joint, and (ii) structures on which muscles attached to the bone may act to generate motion up to some extent. Both of these functions require the bone to be stiff in nature and deform negligibly.

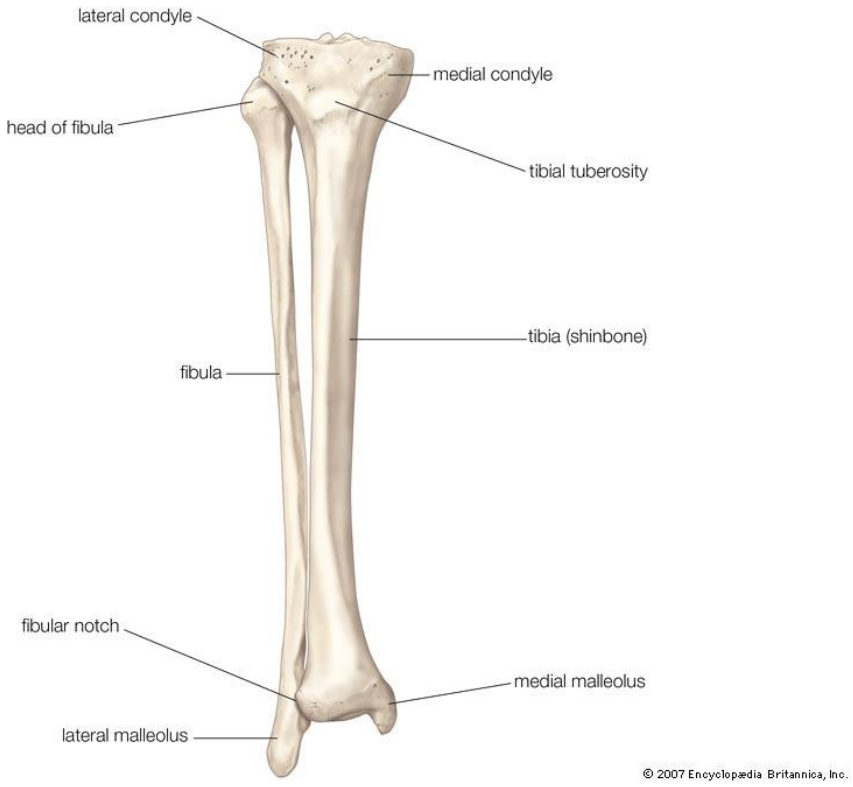

Figure 3.11: Photograph of a typical tibia bone with supporting bones.

When we examined tibia bone at the macroscopic level, long bone consists of two distinct types of bone tissue structure, cortical (compact) and cancellous (spongy or trabecular) tissues. Compact bone tissue is a low porosity and high stiffness dense material in nature and forming the extremely hard outer shell of epiphyseal and the diaphyseal regions of the long bones while the cancellous bone tissue comprises of high porosity and directional dependent stiffness thin plates (trabeculae) in a loose mesh structure enclosed by the cortical bone [38].The periosteum of bone is a dense fibrous membrane that covers the entire bone except joint surfaces which are covered by the articular cartilage. During immaturity, cells of periosteum are generally responsible for circumferential enlargement and remodelling of the growing long bone, hence it is also known as osteogenic layer in bones.

2.4.2 Fibula bone

The fibula bone is a leg bone located on the lateral side of the tibia bone, with which it is connected above and below. It is the smaller of the two bones located, and, in proportion to its length, the slenderest of all the long bones found in human body. Its upper extremity is smaller in size, placed toward the back of the head of the tibia bone, below the level of the knee joint, and excluded from the formation of knee joint. It's (the fibula bone) lower extremity inclines a little forward from normal position, so as to be on a plane anterior to that of the upper end; it projects below the tibia bone, and forms the lateral part of the ankle joint.

The fibula bone does not carry any significant load (weight) of the human body. It extends to past the lower end of the tibia bone and forms the outer part of the ankle joint providing stability to this joint. It has some grooves for certain ligaments which gives them leverage and multiplies the muscle force.

3.0 Biomechanical Behaviour of Synovial Fluid

In human knee joint, Synovial fluid is not isolated from the articular cartilage (AC) but it is interconnected with the residual synovial fluid present in the pores during running, walking etc.

An integrated unit is generated under the load and formed the incompressible 'cushion' which is able to transfer extreme load and protecting the peripheral and the internal articular cartilage structures from their destruction.
First intensive scientist investigates of composition and property of synovial fluid [24, 25, and 26] which were shortly followed by the study of special rheological properties of synovial fluid which were the main chemical constituent if synovial fluid hyaluronan [17, 18].

Synovial fluid provides nutrition articular cartilage. The major constituents of synovial fluid are water, hyaluronic acid (HA), roughly 3-5miligram/ml, and D-glucuronic acid and D-N acetyl glucosamine. It also contains an essential growth hormone prolactin (PRL) and glycoprotein lubricants. Hyaluronic acid – protein complex is responsible for the viscous properties of the synovial fluid. Synovial fluid composition and visual characteristics are strongly dependent on the state of health of the patient without any disorders the normal synovial fluid has egg white like consistency and colour. Synovial fluid is secreted in the cavity by its inner membrane called synovium [29].

Synovial fluid has non linear properties on the peripheral zone of articular cartilage. During mechanical loading, certain amounts of synovial fluid are movable in articular surface and there are changes in synovial fluid viscosity.

The flow of synovial fluid reacts to the magnitude of shear stress and the velocity of human knee joint during rotation of femoral and tibia part when the limbs shift from flexion to extension or vice-versa.

In human joint, articular cartilage is a visco elastic composite biomaterial and its biomechanical function is:

- It helps to transferring the physiological loads into the subcondral bone and the spongious bone.
- It helps lubricate the articular plateaus of joints.
- It protects the articular cartilage surface from high physiological load.

In the peripheral zone of knee joint, the macromolecule structure of articular cartilage has some fundamental biomechanical functions:

- To maintain the lubrication at the articular cartilage at knee joint
- To protect the chondrocytes and extracellular matrix from high loading

Synovial fluid present between the opposite surfaces of articular cartilage has non homogenous property. Its properties not only depend on loading but depend on its life time. During loading viscosity of the synovial fluid greatly varies. Synovial fluid is a viscous pseudo plastic non Newtonian fluid. Apparent viscosity of the synovial fluid decreases with the increasing of shear rate (velocity gradient). It is thixotropic fluid which generally does not display a decrease in viscosity over a time of constant flow of velocity gradient.

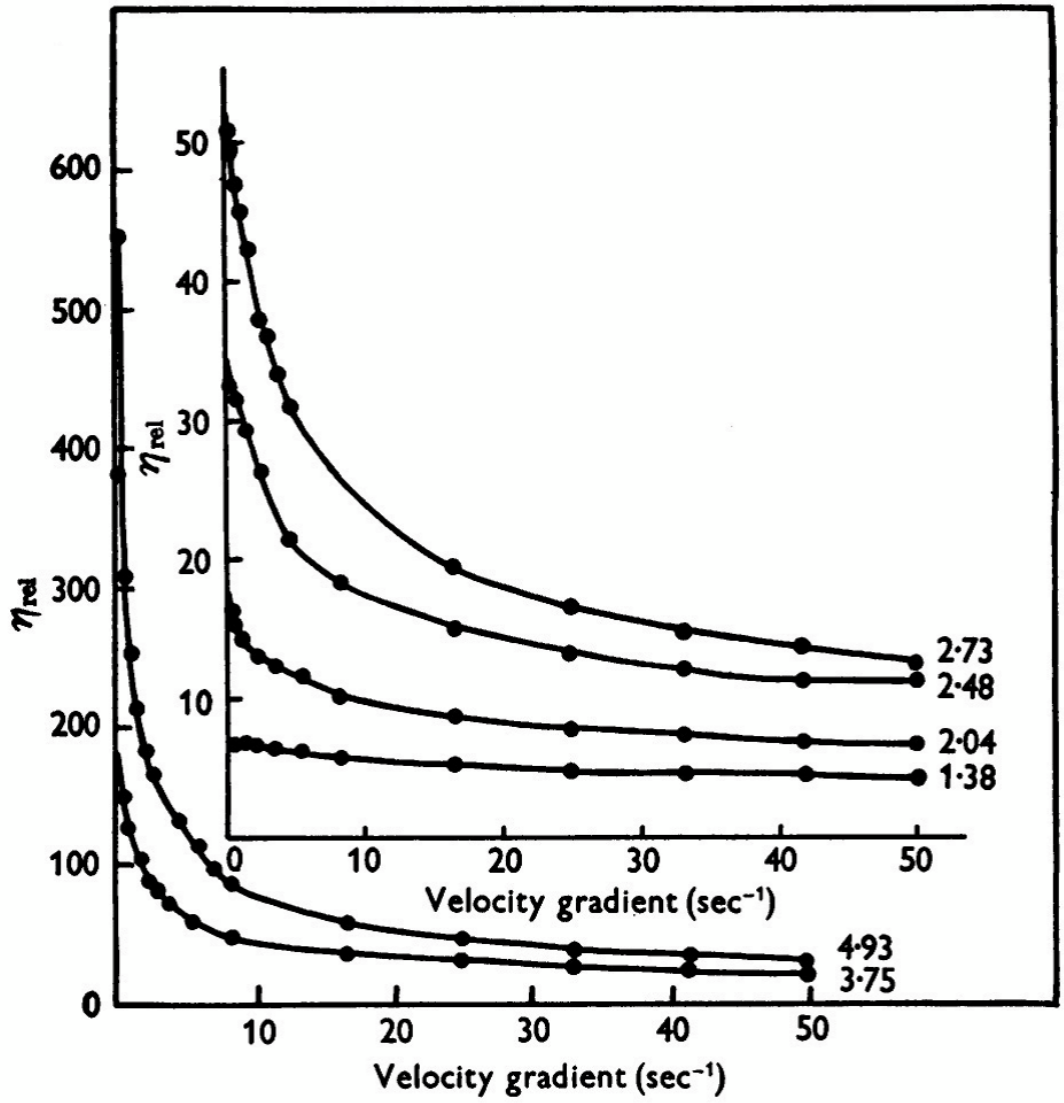

Fig.2.2: (c): Shear – thinning experiment on synovial fluid over a wide range of physiological concentration of the hyaluronan. The relative viscosity against the velocity gradient, Viscosity was measured in the Couette viscosimeter [18].

Figure3(c) shows, when the shear rate (velocity gradient) of synovial fluid increases then the decreases in viscosity of synovial fluid. The change in velocity (Δv) in synovial fluid is the product of thickness (t) of aritcular cartilage surface of the synovial joint and shear rate (γ) of synovial fluid.

$$\Delta v = t * \gamma \qquad (6)$$

In vortex flow, when a flowing synovial fluid passes through the slender structure, it separates and moves around the object. Here, the structure of the bone can be considered as a slender structure. At the point of contact with the structure, vortex swirls separate from the body on alternating sides. This separation causes local increase in pressure and a decrease in velocity on one side and, also decrease in pressure and an increase in velocity on the opposite side. The alternating velocities

generate alternating pressure forces on either side of the bluff object. The frequency of these pressure changes is proportional to the velocity.

In fluid dynamics, vortex shedding is an oscillating flow that takes place when a fluid such as air or water flows past a bluff (as opposed to streamlined) body at certain velocities, depending on the size and shape of the body. In this flow, vortices are created at the back of the body and detach periodically from either side of the body. See Von Karman Vorte Street. The fluid flow past the object creates alternating low-pressure vortices on the downstream side of the object. The object will tend to move toward the low-pressure zone.

The periodic vortex shedding 'f' is proportional to velocity 'v'.

The frequency at which vortex shedding takes place for a cylinder is related to the Strouhal number by the following equation:

$$\mathrm{St} = \frac{fD}{V}$$

Where St is the Strouhal number, f is the vortex shedding frequency, D is the diameter of the cylinder, and V is the flow velocity.

The Strouhal number depends on the body shape and on the Reynolds number.

Strouhal number is the ratio between interval of the vortices and the shedder bar width. Since the shedder bar width is fixed, due to this reason the Strouhal number to remain constant and the vortex interval must also be held at constant. This interval remains constant when the pipe Reynolds number is within a certain range.

Range of Reynolds number will vary with the size and shape of the body from which eddies are being shed, as well as with the kinematic viscosity of the fluid. The Strouhal number is the ratio between the vortex interval and the shedder bar width. Usually for such cases, the vortex interval is about 6 times the shedder bar width for given sample. While, Strouhal number is the reciprocal value (~0.17).

Vortex induced vibration among macromolecules which will lead to fatigue failure of articular surface of the knee joint. When a fluid flows over a contour line of articular cartilage surface of the knee joint there is formation of Karman vortex shedding. This bone structure will vibrate across the line of fluid flow direction and this cross fluid flow vibration would become severe if frequency of periodic vortex shedding matches with the natural frequency of the structure. Corresponding ranges of fluid velocity across joints are called critical velocity.

4.0 Fatigue Failure

Fatigue fractures and wear have been identified as some of the major problems associated with implant loosening, stress shielding and ultimate implant failure [9, 13]. Due to repeated loading below the bone's ultimate strength, micro structural damage occurs. When muscles become fatigue and significantly less able to counter act load during continuous strenuous physical activity, progressive loss of strength and stiffness causes this type of damage. Crack begins at discontinuities within the bone tissues (e.g. haversian canals, lacunae). This should be affected by the magnitude of the load, number of cycles and frequencies of loading process.

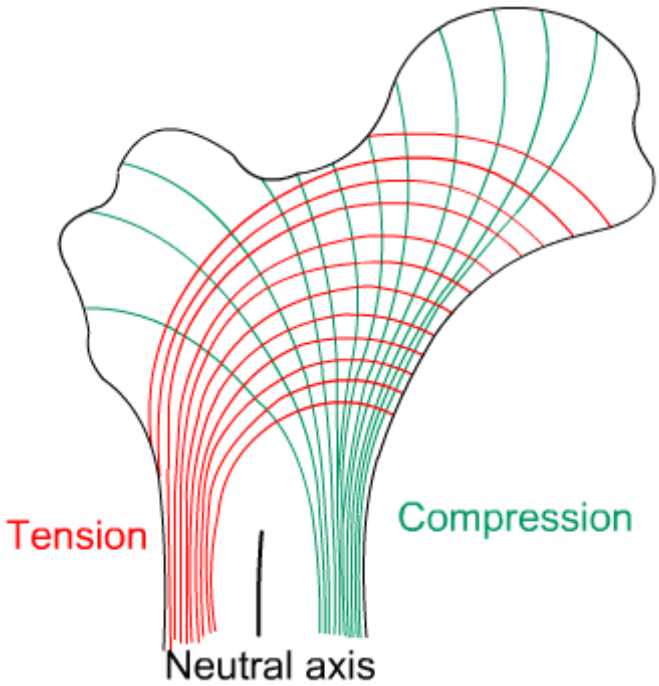

Fig.3.12: Cortical region of bone showing tension and compression in load condition

There are following three stages of fatigue failure:

Crack initiation:

- It is a result of discontinuities which increased local stress where micro cracks form. By using remodelling of bone, repairs these cracks.

Crack growth (propagation):

- If the micro cracks are not repaired and grows until they encounter a weaker material surface and change direction of micro crack. Transverse growth is stopped when the generated crack turns from perpendicular to parallel to the load.

Final fracture:

- It occurs only when the fatigue process progresses faster than the rate of remodelling.

There are three region in which the process of fatigue failure shows:

Region 1:

First Region consist crack initiation, accumulation and growth. Its characteristics are at high stress concentration and low strength region matrix damage. In this, loss of stiffness starts rapidly. It bear less load and absorb more energy (sustain larger deflection) and because of this, cracks develops rapidly. It may be stabilize quickly without much propagation. Cracks occur in high strain region and when it accumulate and increased by number of cycles and strain. Cracks develop perpendicular to the load axis.

Region 2:

This region includes crack growth (expand horizontally), coalescence and delamination debonding. When crack forms, interlamellar tensile and shear stresses are generated at its tip. Then, it tends to separated and shear lamellar at the fibre matrix interface.

Secondary cracks growth between the lamellar in the load direction. Crack grows parallel in the load direction.

Region 3:

In this, stiffness declines rapidly and it is the end of material's fatigue life span. It is a rapid process and ultimate failure of the structure.

For fatigue failure two parameters are important. One is stress amplitude and another one is load cycle analysis.

Load cycle analysis can be carried out from S-N curve for the knee joint. Expected number of stress cycles in the projected working life of a structure is related to expected number of hours load per year in the critical velocity range.

Stress fractures are partial or complete fracture of bone and it is repetitive strain during sub maximal activity. There are two main types:

- Fatigue fracture
- Insufficient fracture

Fatigue fracture may be caused by:

Abnormal muscle stress:
It may be loss of shock absorption or may be repeated activity.

Torque:
In this, bone with normal elastic resistances.

Fatigue fracture caused by abnormal loading or abnormal stress distribution.
In fatigue failure, it has been observed that material fail under fluctuating stresses at a stress magnitude which is lower than the ultimate tensile strength of the material. Sometimes, the magnitude is ever lower than the yield strength. Further, it has been found that the magnitude of the stress that causes fatigue failure decreases as the number of stress cycles increases. This phenomenon of decreased resistance of the material of fluctuating stresses is the main characteristics of fatigue failure.

In case of failure under static load, there is sufficient plastic deformation prior to failure, which gives a warning well in advance. On the other hand fatigue cracks are not visible till they reach the surface of component and by that time; the failure has already taken place. The fatigue failure is sudden and total.

S-N curves represent range of data pairs, each representing the number of cycles (N) of a constant stress range (S) that will cause fatigue failure. A series of fatigue tests are made on a number of specimens of the material at different stress levels. The stress endured is then plotted against the number of cycles sustained. It is the graphical representation of stress amplitude versus the number of cycles before the fatigue failure.

S-N curve is a standard method of presenting fatigue data. In S-N curve, a stress level below which the material sample will theoretically withstand an infinite number of stress cycles without fracture. This stress value is called the fatigue limit of the material or the endurance limit. To determine the endurance limit a number of tests are to be carried out. In true sense endurance limit is not exactly property of material like ultimate tensile strength. It is affected by the factors such as the size and shape of the component, surface finish, and temperature and notch sensitivity of the material. S-N curve for an idealized metal and for cortical bone show a marked difference in fatigue behaviour.

Fatigue life is governed by loading in three interval ranges as follows:

- Low life Region, i.e. under large stress cycles, fatigue life cycles is less than about 10^4 cycles.
- Medium life Region, with fatigue lifecycles is from 10^4 to 10^6 cycles.
- Long life Region, When under low stress cycles, Fatigue life is greater than 10^6 cycles.

For design of finite life, the endurance limit criterion of failure is the stress amplitude should be lower than the expected endurance limit in order to withstand the infinite number of cycles.

5.0 Weibull distribution

Weibull distribution method is one of the most widely used lifetime distribution in reliability engineering due to its versatility. Weibull distribution function has been commonly used in many fields including life length analysis of material and to analyze fracture strength data of brittle material.

The primary advantage of weibull analysis process is the ability to provide reasonably accurate failure analysis and failure forecasts with extremely small samples. It also provides a simple and useful graphical picture of the failure data.

Weibull distribution is a three parameter probability distribution method. The PDF (probability Distribution function) of Weibull distribution is given by the mathematical formula as follows:

The probability density function of a given Weibull random variable is:

$$f(x;\lambda,k) = \begin{cases} \frac{k}{\lambda}\left(\frac{x}{\lambda}\right)^{k-1} e^{-(x/\lambda)^k} & x \geq 0, \\ 0 & x < 0, \end{cases}$$

Where $k > 0$ is the *shape parameter* and $\lambda > 0$ is the *scale parameter* of the distribution. Its complementary cumulative distribution function is a stretched exponential function. The given Weibull distribution is related to a number of other probability distributions; in the given particular, it interpolates between the exponential distribution of equation ($k = 1$) and the Rayleigh distribution ($k = 2$ and $\lambda = \frac{\sqrt{2}}{k}$).

If the quantity *X* is a "time-to-failure", the given Weibull distribution for which the failure rate is proportional to a power of time. The given *shape* parameter, *k*, is that power plus one.

'V' is the velocity of synovial fluid, 'k' is the non dimensional shape parameter,'s'is the scale parameter and 'ε' is the location parameter. The dimension of 'ε' and 's'are same as of 'v'.

The location parameter 'ε' is the velocity of synovial fluid and $v \geq \varepsilon$. The CDF (Cumulative distribution function) method is given by integrating the equation which is:

$$F(x;k,\lambda) = 1 - e^{-(x/\lambda)^k}$$

for $x \geq 0$, and $F(x; k; \lambda) = 0$ for $x < 0$.

The quantile (inverse cumulative distribution) function for the Weibull distribution is

$$Q(p;k,\lambda) = \lambda(-\ln(1-p))^{1/k}$$

For $0 \leq p < 1$.

The failure rate *h* (or hazard function) is given by

$$h(x;k,\lambda) = \frac{k}{\lambda}\left(\frac{x}{\lambda}\right)^{k-1}.$$

Since, the value of location parameter of velocity of synovial fluid is small, it can be equate to zero. By taking ε=0 three parameter Weibull distribution comes to two parameter Weibull Distribution method. The probability Distribution Function is-

$$P_u = P_x \left|\frac{\partial x}{\partial u}\right|.$$

The CDF of a continuous random variable *X* can be expressed as the integral of its probability density function f_X as follows:

$$F_X(x) = \int_{-\infty}^{x} f_X(t)\,dt.$$

If 'v' is the velocity of synovial fluid, k and s are the Weibull distribution parameter, then mean and variance of the Weibull Distribution are given by the following experiment:

$$F(x) = \mathrm{P}(X \leq x) = \sum_{x_i \leq x} \mathrm{P}(X = x_i) = \sum_{x_i \leq x} p(x_i).$$

Where 'm' is the mean, 'σ' is the standard deviation of velocity of synovial fluid and is the gamma function.

The parameter in the distribution provides a great deal of flexibility to model systems in which the number of failure increases with time (bearing wear) and decreases with time (some semiconductor), or remains constant with time (failure caused by external shocks to the system) [20].

6.0 Material and method

Curve between normal stress and velocity gradient of synovial fluid taken.

Table 1.3 gives the data of rate of shear and normal stress at knee joint due to the flow synovial fluid [21].

Shear rate (sec-1)	Normal stress (Pa) (peak values)
90	420
142	1020
285	3630
450	9180
900	15000
1420	31000
2850	68000
4500	106000
9000	200000

Table 1.3: Knee-peak values between rate of shear and normal stress [21].

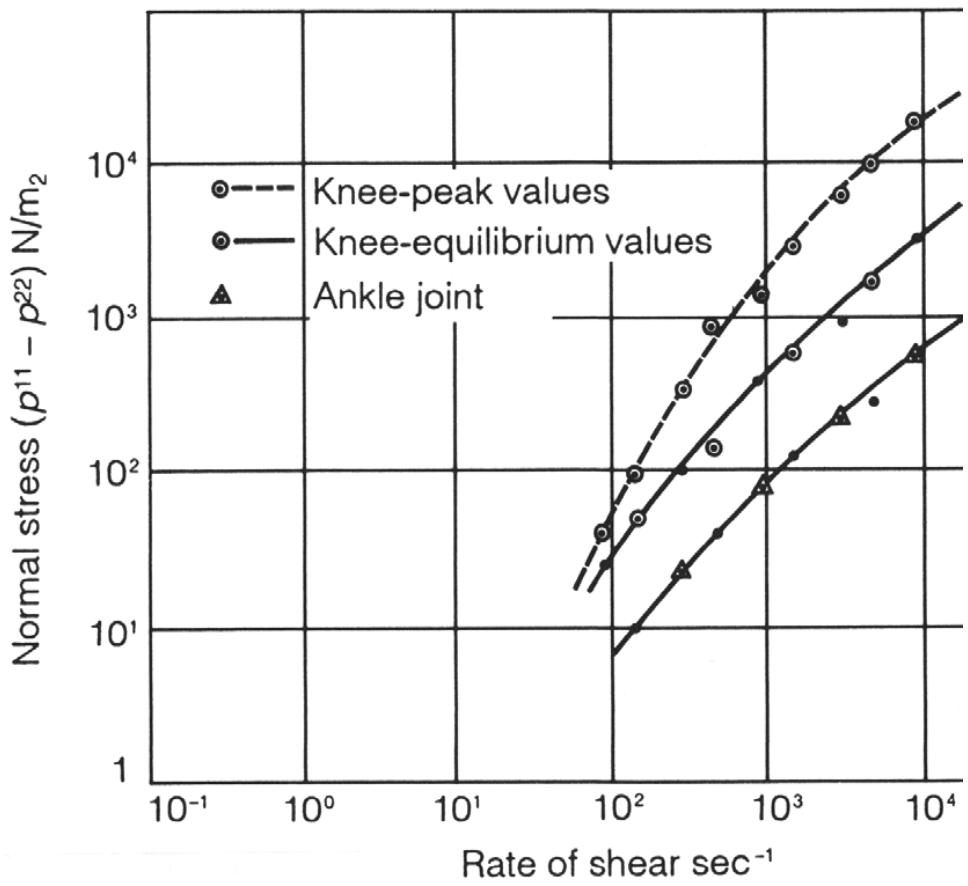

Figure 2.3(a): shows differences as function of shear rate. Two sample of bullock's synovial fluid (from ankle and knee) were tested in the Weissenberg rheogoniometer. The plot shows the peak values developed within few seconds after beginning of experiment. Then the normal stress differences fell and reached the equilibrium values (after approx. 50 seconds). In the case of the ankle joint, the differences between peak and equilibrium values were not significant and thus the peak values are not plotted [21].

The total thickness of the gap between the opposite articular surfaces is only 50 µm; including height Roughness of the surfaces near both peripheral layers 2x 2.5 µm [22].

.

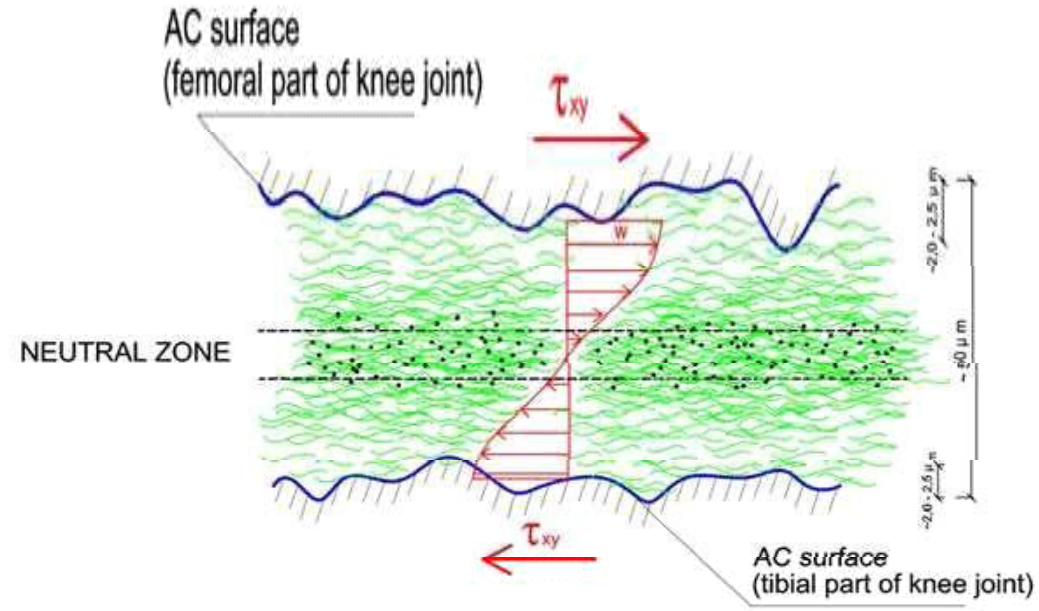

Figure 2.4(b): Distribution of magnitude and direction of synovial fluid flow velocity vectors in the gap between articular surfaces. Associations of NAHA/HA macromolecules decline in places with the greatest SF flow velocity gradient, i.e. in zone adjoining each AC surfaces. The SF flow velocity gradient decreases in the direction towards the neutral zone [22].

Averages radiuses of condyler curves were between 4.5cm & 1.7cm medially and between 3.2cm &1.8cm laterally for 00 and 900 flexion contacts respectively. For intercondylar width was 2.20cm +0.18cm [11]. It varies person to person.

Average diameter of both (medially and laterally) =11.2cm

Average diameter of intercondylar = 2.20cm

Total average diameter of condoylar (medial, lateral and intercondylar) = 13.4cm or 0.134m [23].

For typical running speeds (3-5m/s), K_{leg} is on the order of 10KN/m and varies relatively little with speed [24, 25, 26].

Mass of the lower leg is 7.5% of the total body weight. In this thesis, assume a person weight is 80Kg and 120Kg [27].

Strouhal number is the ratio of shedder bar width and vortex interval. Usually vortex interval is 6 times of the shedder bar. So, Strouhal number is approx 0.17.

6.0 Result and Discussion

The objectives of decipher was to check up the calculation of stress cycles in the service life of knee joint by determining the required count of hours per year in baleful velocity ranges.. The fatigue strength of the bone is due to fatigue caused by the vortex shedding of synovial fluid, statistically through the weibull distribution. The probability distribution of sample according to which the bone will fail was obtained and the reliability of the bone under such instance was examined. The relationship between the fracture strength and the flow of velocity of the synovial fluid was deduced by the S- N curve. The results obtained are given as follows:

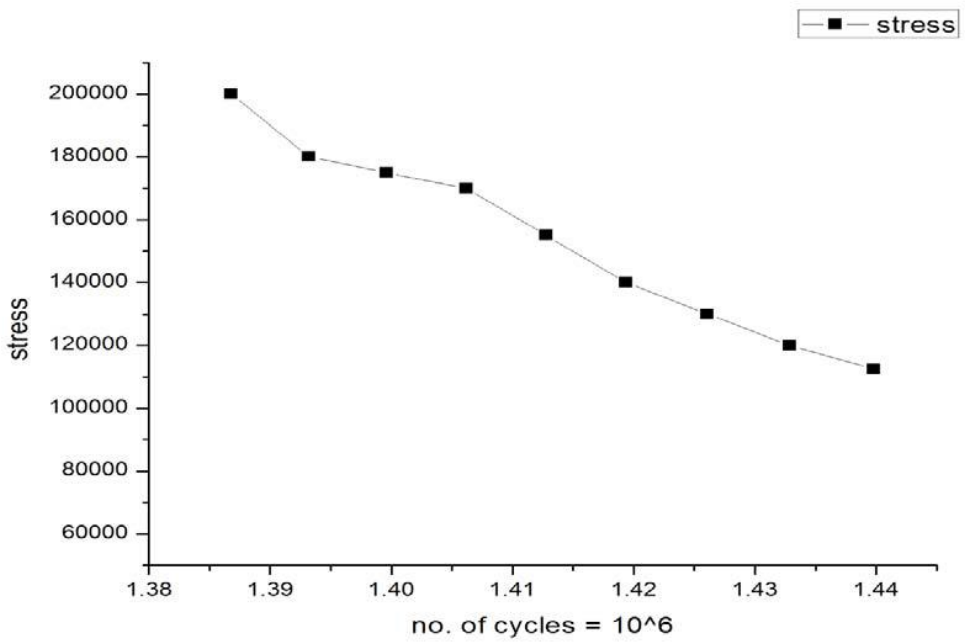

Fig. 2.5(a): S-N curve (knee joint)

Number of cycles (10^6)	Stress(Pa)
1.4398	112500
1.4329	120000
1.4261	130000
1.4194	140000
1.4128	155000
1.4062	170000
1.3996	175000
1.3932	180000
1.3868	200000

Table 1.4: Calculated Number of stress cycles against stress amplitude to plot a S-N curve (knee joint)

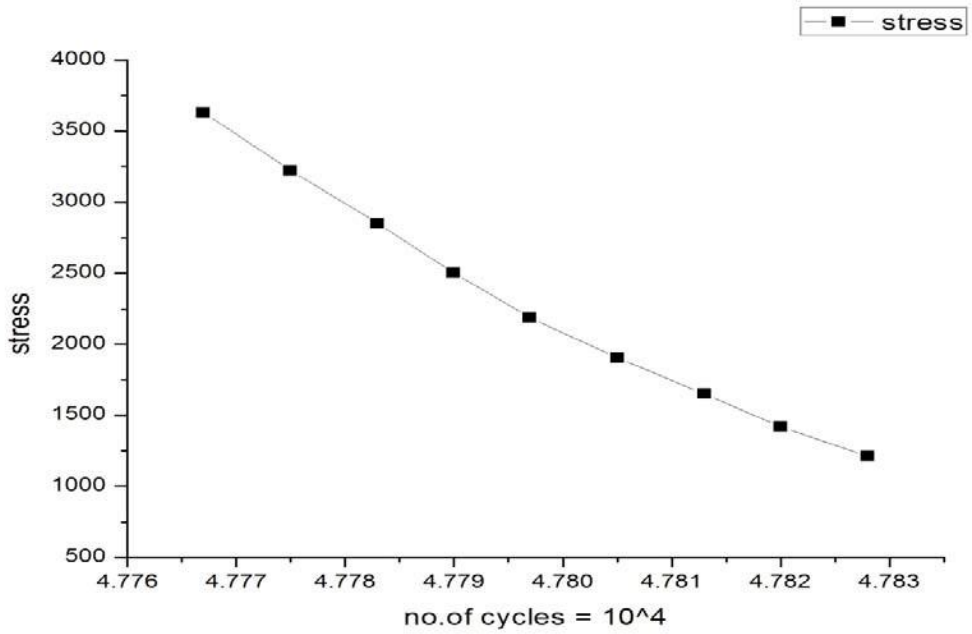

Fig. 2.6(b): S-N curve (knee joint)

Number of cycles (10^4)	Stress(Pa)
4.7828	1211
4.7820	1420
4.7813	1650
4.7805	1905
4.7797	2188
4.7790	2501
4.7783	2850
4.7775	3221
4.7767	3630

Table 1.5: Calculated no. of stress cycles against stress amplitude to plot an S-N curve (knee joint)

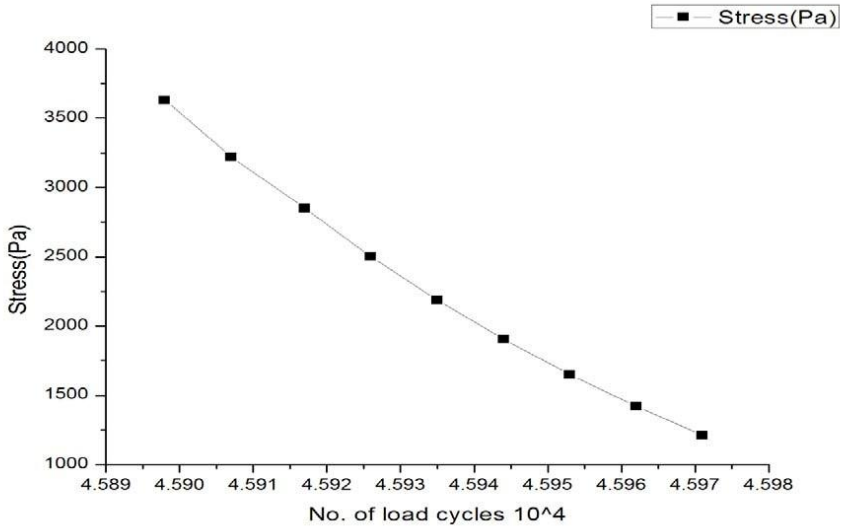

Fig.2.6(c): S-N curve (knee joint)

Number of cycles (10^4)	Stress(Pa)
4.5971	1211
4.5962	1420
4.5953	1650
4.5944	1905
4.5935	2188
4.5926	2501
4.5917	2850
4.5907	3221
4.5898	3630

Table 1.6: Calculated no. of load cycles against stress amplitude to plot an S-N Curve (knee joint)

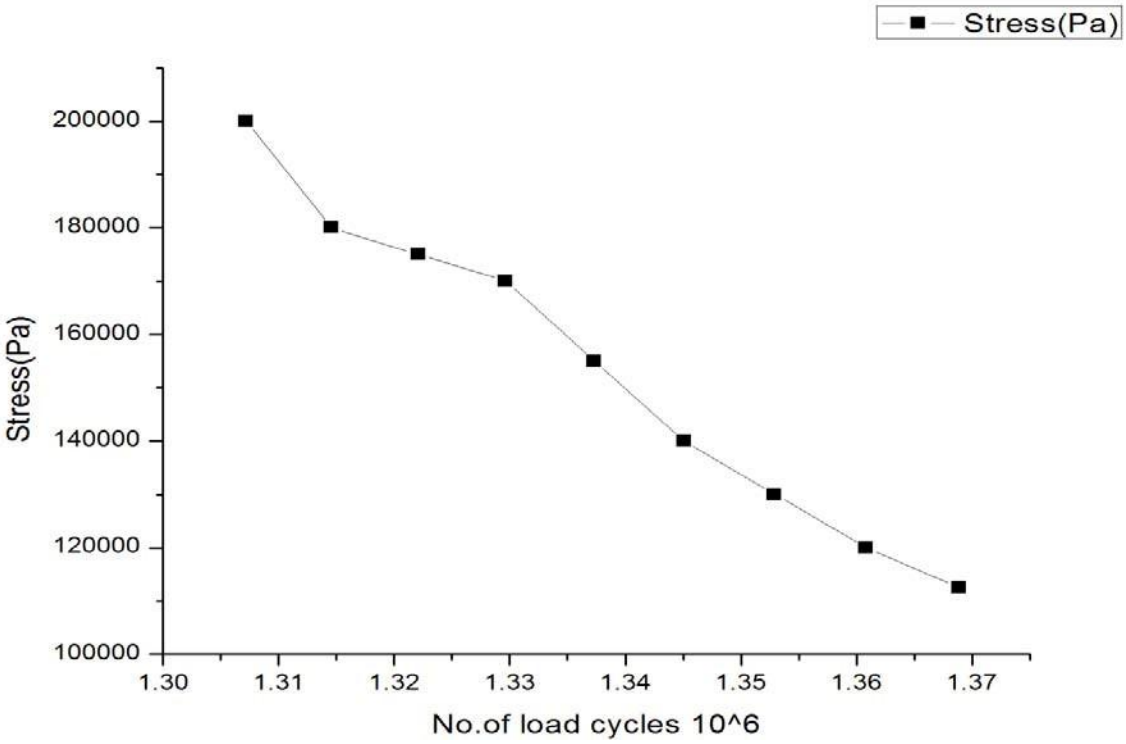

Fig 2.7(d): S-N curves (The knee joint)

Number of cycles (10^6)	Stress(Pa)
1.36887	112500
1.36085	120000
1.35291	130000
1.34507	140000
1.33732	155000
1.32965	170000
1.32208	175000
1.31459	180000
1.30718	200000

Table 1.7: Calculated no. of load cycles against stress amplitude to plot S –N curve (knee joint)

Fig.2.6 (a) to fig.2.7 (d) show the S-N curve at different velocities of synovial fluid to determine the fracture strength of the articulating surfaces in knee joint due to cyclic loading. Calculation of load cycles was quantified by proceeding the formula as given.

Where N is the count of stress cycles, and 'T' is the total number of hours in the time period over which stresses act on the articular cartilage surface of the knee joint, 'T' is that particular time period over which the natural frequency of the bone structure matched with the recurrent vortex shedding repetition of the synovial fluid. 'F' is the cumulative probability of the velocity distribution of synovial fluid. Table no. 1.4 to Table no. 1.7 shows the stress amplitude of which the number of stress cycles has been calculated.

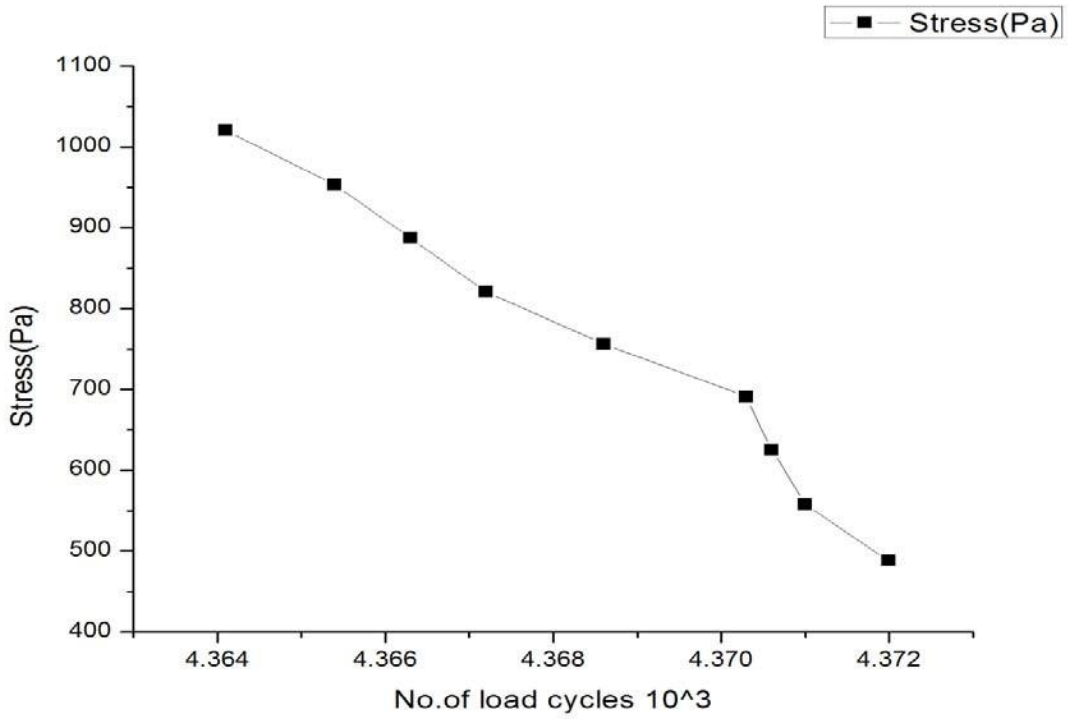

Fig 2.8 (e): S-N curves (Knee joint)

No of cycles (10^3)	Stress (Pa)
4.372	488
4.371	559
4.3706	626
4.3703	692
4.3686	757
4.3672	822
4.3663	887
4.3654	953
4.3641	1020

Table 1.8 Calculated no. of load cycles against stress amplitude to plot an S-N curve (knee joint)

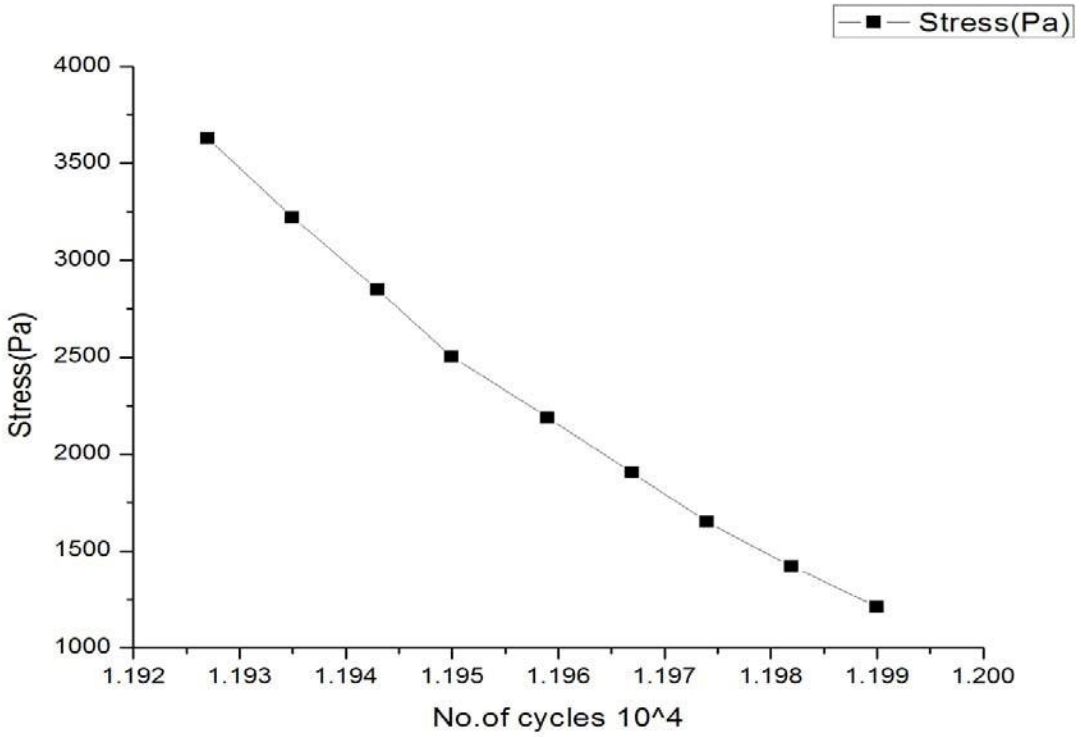

Fig. 2.9(f): S-N curve (knee joint)

No of cycles (10^4)	Stress
1.1990	1211
1.1982	1420
1.1974	1650
1.1967	1905
1.1959	2188
1.1950	2501
1.1943	2845
1.1935	3221
1.1927	3630

Table 1.9 Calculated no. of load cycles against stress amplitude to plot an S-N curve (knee joint)

Case I:

Fig. 2.6 (a) to Fig. 2.6 (b) showed the S-N curve of the normal weight person (80kg) whose natural frequency of the bone structure was 6.5cycles/sec.

Fig.2.6 (a) shows, the stress value was 200000Pa then count of the likely load cycles was 1.3878*105 and at 112500Pa load expected count of load cycles was arises as 1.4396*104 in optimised conditions. In this situation, the velocity of the synovial fluid lies in the range of 5.225 m/sec to 5.45m/sec.

In Fig.2.6 (b), at 3630Pa the number of stress cycles was $4.7767*10^4$ and at 1211Pa the number of stress cycles was 4.7828*104. The velocity of synovial fluid lies in the range of 5.0071m/sec to 5.01425m/sec.

Case II:

Fig. 2.6 (c) to Fig. 2.7(d) showed the S-N curve of the normal weight person (120kg) whose natural frequency of the bone structure was 5cycles/sec.

Fig.2.8 (e), at 1020Pa the number of stress cycles was $4.3641 *10^3$ and at 488Pa the number of stress cycles was $4.372*10^3$. The velocity of synovial fluid lies in the range of 2.5045m/sec to 2.5071m/sec.

In Fig.2.9 (f), at 3630Pa, expected count of stress cycles was $1.1912*10^4$ and 1211 Pa the possible output count of stress cycles was $1.1980*10^4$. The velocity of synovial fluid lies in the range of 2.5071m/sec to 2.51425m/sec.

In Fig 2.6 (a) to Fig 2.9 (f) follows the S-N curve. At different critical velocities of the synovial fluid in the knee joint, the possible count of load cycles which is lies in the range from 10^4 to 10^6 scale, that increases with the decreasing in stress dimension values which results, the resultant curve was exponentially decreases. At lower stress value the articular surface bear the high stress and as the number load cycles increases then the stress bearing capacity of the articular surfaces of the knee joint decreases.

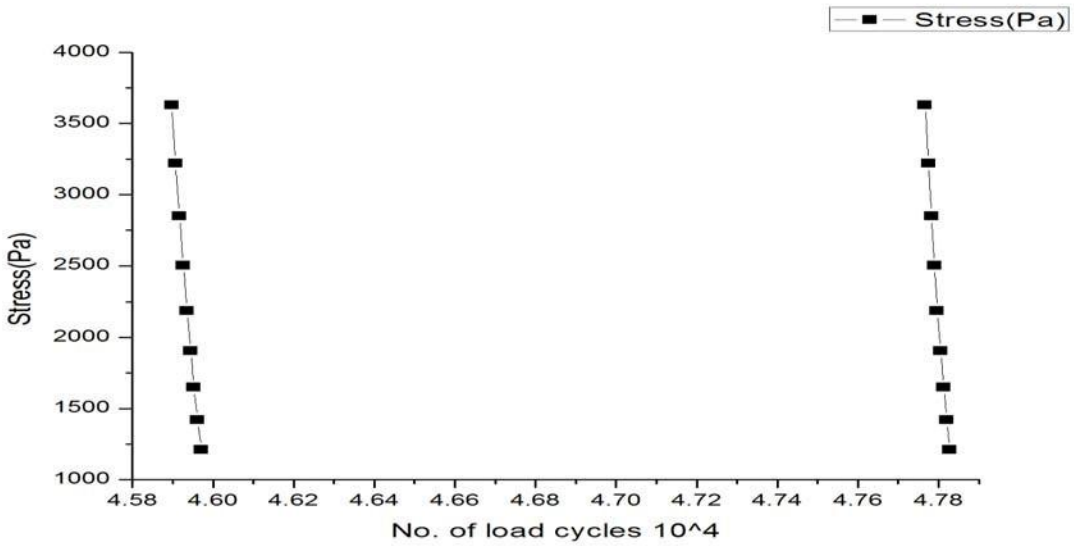

Fig 2.10(g): S-N curve of the different weighted person at the same stress values (knee joint)

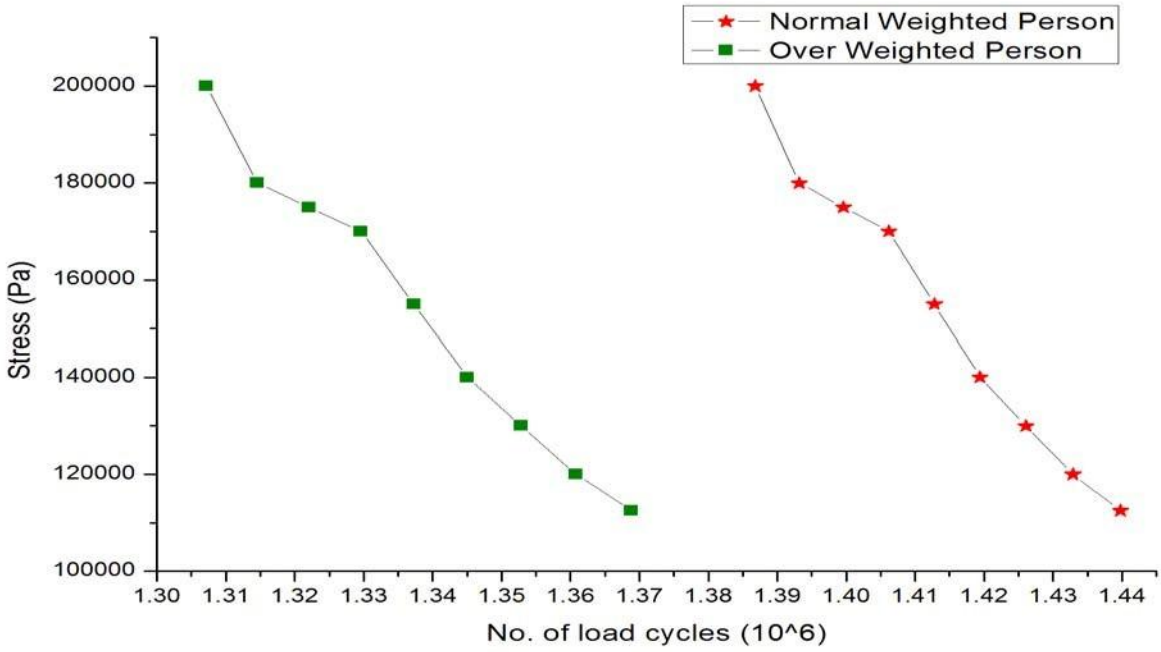

Fig 2.11 (h): S-N curve of the different weighted person at the same stress values (knee joint)

Fig 2.10(g) and fig 2.11 (h) show the same stress amplitude but their number of stress cycles is different which depend on the weight of the person. The S-N curve on the left side shows the fatigue failure of the knee joint of the overweighed person (120kg) and right curve shows the fatigue failure of the knee joint of the normal

weight person (80kg). In overweighed person, fatigue failure in the knee joint occur at less number of stress cycles as compared to the normal weight person when the stress amplitude was same.

Each stress value shows its respective number of stress cycles and when the possible count of stress cycles increases, the resultant fatigueness take place in the articulating surface of the knee joint of bone. It is also shown the fatigue life of the structure.

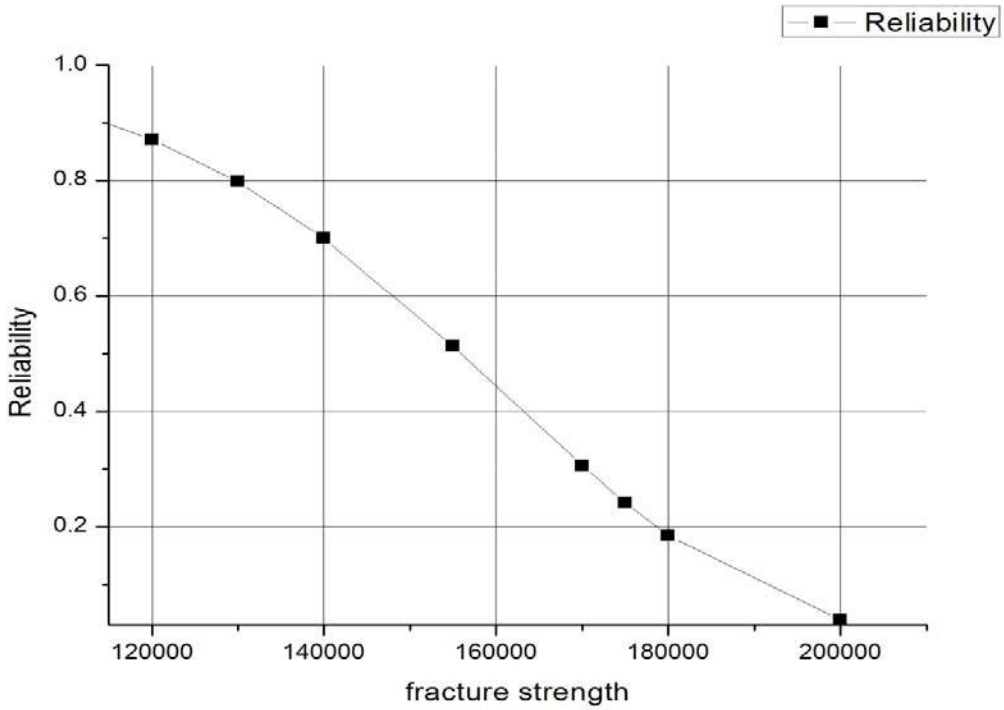

Fig. 2.12(i): Weibull reliability distribution curve (k=6.1902 & s=165430 Pa).

Fracture Strength (Pa)	Reliability
112500	0.912
120000	0.871
130000	0.798
140000	0.700
155000	0.513
170000	0.306
175000	0.242
180000	0.185
200000	0.039

Table 1.10: Calculated reliability at different stress values (k=6.1902 & s=165430 Pa).

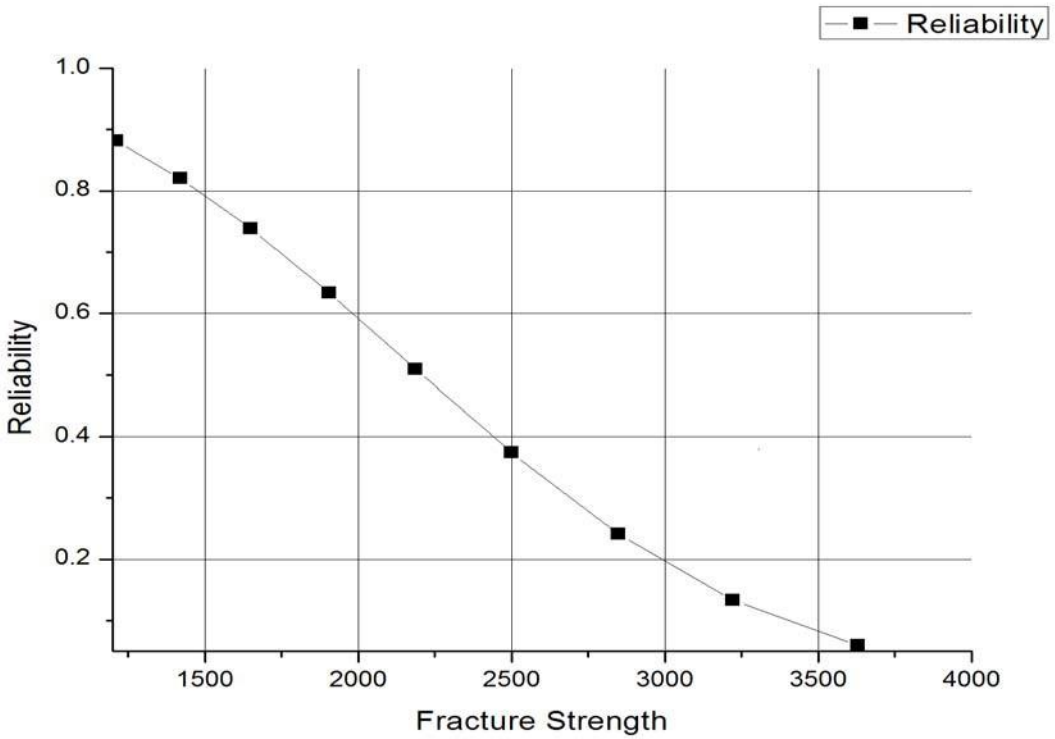

Fig 2.13(j): Weibull reliability distribution curve
(k=2.8289 & s=25155.5 Pa)

Fracture Strength(Pa)	Reliability
1211	0.8811
1420	0.8199
1650	0.7382
1905	0.6339
2188	0.5094
2501	0.3736
2850	0.2406
3221	0.1335
3630	0.0593

Table 1.11: Table contain the reliability at different stress values (k=2.8289 & s=2515.5 Pa).

The variation of the fracture strength of the bone was modeled using the weibull distribution. For Weibull reliability distribution, using the stress values which are given in Table 1.8 and Table 1.9. The Weibull distribution was determined. The shape parameter and scale parameters of weibull distribution were determined using Maximum likelihood method. For the Table 1.8 the estimated shape and scale parameter was 6.902 and 165430 (Pa) respectively and for Table 1.9 the estimated shape and scale parameter was 2.7289 and 2515.5 (Pa) respectively. The reliability at different stress values was calculated and shown graphically. Table shows the reliability of the bone at different stress values. Fig.2.8 (e) and given Fig.2.9 (f) shows the reliability curve for the same. Generally at higher stress value, this result may also arise and the reliability will be least and at lower stress value, the reliability will be high.

7.0 Conclusion and future scope

7.1 Concluding Remarks

Weibull statistics was used to determine the possible count of hours per year in baleful velocity range of synovial fluid. It lies in the range where the resonant frequency of the knee joint matched with the frequency of periodic vortex shedding of the synovial fluid present in joints. In knee joints, the fatigue failure arises in articular cartilage surface of in human being is shown by S-N curve where the stress level decreases with the possible enhancement count of load cycles.

So we can say that as the person ages, the number of load cycles increases due to running, walking or any other movement and the stress amplitude decreases. As a result, at low stress value there was a fatigue in bone structure.

Here, the other aspect of fatigue failure in the knee joint is weight. In that case the overweighed person has a lower flow of velocity of synovial fluid in the knee joint as compared to the normal weighted person. So the chances of fatigue failure in the knee joint of overweighed person are higher than the normal weighted person.

It was seen that an increase in fracture strength of the bone decreases the reliability. Reliability was highest at least fracture strength and at the higher value of the fracture strength of the bone, reliability approaches to zero. This was shown by the graphical representation of weibull reliability distribution.

7.2 Future Scope

The stress analysis done can be used to design knee and hip orthopaedic prosthetic implant where fatigue failure of the implants remains the major challenge. The fracture strength of the bone determined from the weibull reliability curve can be used as the design stress of the implant devices and can be tested to give better chances of survival of the implant under loading conditions. Also, the stress determined from the S-N curve can be used to design person specific implants depending on their age and weight to sustain failure due to cyclic loading.

8.0 References

1) www.humankinetics.com
2) X.Fan, E.D.case, F.Ren, Y.Shu, M.J.Baumann. "Porosity dependence of the weibull modulus for hydroxyapatite and other brittle materials," Journal of the Mechanical Behavior of Biomedical Material. 21-36, 8(2012).
3) M.F.Burrow, D Thomas, M.V.Swain, M.J.Tyas."Analysis of Tensile Bond Strength Using Weibull Statistics, "Biomaterials 2004.
4) M.S.Zand, S.A.Goldstein and L.S.Mathews "fatigue failure of cortical bone screws," Journal of Biomechanics, Volume 16, No.5, pp.305-311, 1983.
5) P. bhuanantanondh, D.Grecov, E. kwok, "Rheological study of viscosupplements and synovial fluid in patient with osteoarthritis," Journal of Medical and Biological Engineering, 32(1), 12-16, 2010.
6) R.Blickhan, "The Spring Mass Model for Running and Hopping," Journal of Biomechanics, Volume 22, No.11/22, pp.1217-1227, 1989.
7) M.Husriu Dirikolu, A.Aktas, B. Bivgoren, "Statistical Analysis of Fracture Strength of Composite Materials Using Weibull Distribution," Turkish Journal Enigineering Environment Science, 45-48, 26 (2002).
8) R. J. Morrissey, D. L. McDowell, T. Nicholos, "Frequency and stress ratio effects in high cycle fatigue of Ti-6Al-4V," International Journal of fatigue, 679-685, 21 (1999).
9) S. H. Teoh, "Fatigue of Biomaterial: a review," International Journal of Fatigue, 825-857, 22 (2000).
10) G.M. Williams, E.F. Chan, M.M.T. Wong, W.C.Bae, K. Masuda, W. D. Bugbee, R.L. Sah. "Shape, Loading and Motion in the Bioengineering design, Fabrication and testing of Personalized synovial joints," Journal of Biomechanics, 156-165, 43 (2010).
11) M.Biscevic, M.Hebibovic, D.Smrke, "Variations of femoral condyle Shape," Coll. Antropol. Original Scientific paper; UDC 572, 781.087, 2,409-414, 29 (2005).
12) Dumbleton, J.H., "Lubrication of natural joints," Tribology of Natural and Artificial joints, Series 3, 1981.
13) St John KR, "Particulate debris from medical implant," American Society of testing and material, 1992.
14) Meyer, K., Smyth, E., and Dawsen, "The isolation of mucopolysaccharide from Synovial fluid," Journal of Biological Chemistry, (128), 1-319, M. (1939).
15) Ropes, M., Rossmeisl, E., and Bauer, "The origin and nature of normal human Synovial fluid," J. Clin Invest, 50, 795-799, W. (1940).
16) Davies, "Synovial membrane and synovial fluid of joints," Lancet, 7(2), 815-819, D. (1946).

17) Subald., "Studies on hyaluronic acid in synovial fluids," Acta Societatis Medicorum upsaliensis, 58(113), L.(1953).
18) Ogston, A. and Stainer, "The physiological function of hyaluronic acid in synovial fluid, viscous, elastic and lubricant properties," The Journal of physiology, 119 (2-3), 244, J. (1953).
19) Coleman, P.J., Scott, D., Ray, J.,Mason, R.M., Levick, J.R, "Hyaluronan secretion into the synovial fluid of rabbit knees and comparison with albumin turnover," The Journal of Physiology, 503, 645-656, 1997.
20) D. C. Montgomery, G. C. Runger, "Applied Statistics and Probability for Engineers," 193-194; 1999.
21) King, R.G, "A Rheological Measurement of three Synovial Fluids," Rheologies Acta, 5(1), 41-44, (1966).
22) Petryl, M., Bastl, Z., Hulejova, H., Polauska, M, Lisal, J., Danesove, J.& cerny, "Cycloolifin-copolymer/polyethylene (COC/PE) Blend assists with the caution of New Articular Cartilage macromolecular symposis special tissue, Layered Nanosturctures-Polymers with Improved Properties," Volume.294, No.1, pp.120-132, 1 August 2010.
23) M. Biscevic, M.Hebibovic & D Smrke, "Variations of femoral condoyle shape, Original scientific paper, UDC 572; 409-414; 29;2005.
24) T. A. Mc Mohan and G.C. Cheng, "The mechanics of Running: How does stiffness couple with speed," Journal of Biomechanics, Volume 23, pp. 65-78, 1990.
25) C. T. Farley and D. P. Ferris, "Biomechanics of Walking and Running: from centre of mass movement to muscle action," Exercise and Sports Science Reviews, Volume 26, pp.253-285, 1998.
26) G. Elliot, G. S. Sawicki, Andrew, Marecki, H.Herr, "Biomechanics and energetic of Human Running using an elastic Knee Exoskeleton," Experimental paper.
27) Kiok, Li, Saybolt, and Tejani., "fracture Analysis," BE-209 Capstone Project.
28) Weibull, W., "A Statistical Distribution function of Wide Applicability,"Journal of Applied Mechanics, 18; 293-297; 1951.
29) http://img.tfd.com/mk/E/X2604-E-41.png
30) http://www.intechopen.com/source/html/18659/media/image8.jpg
31) http://cerebrovortex.files.wordpress.com/2012/03/bone stresstensioncompressioninfemurhead_updated.png
32) http://images.wisegeek.com/diagram-of-anatomy-of-bone.jpg
33) http://blog.drwile.com/wp-content/uploads/2013/03/osteon.jpg
34) Drake, Richard L.; Vogl, A. Wayne; Mitchell, Adam W. M. (2010). Gray´s Anatomy for Students (2nd Ed.). pp. 584–588. ISBN 978-0-443-06952-9.

35) Rytter S, Egund N, Jensen LK, Bonde JP (2009). "Occupational kneeling and radiographic tibiofemoral and patellofemoral osteoarthritis". J Occup Med Toxicol (1): 19. Doi: 10.1186/1745-6673-4-19. PMC 2726153. PMID 19594940.
36) Gill TJ, Van de Velde SK, Wing DW, Oh LS, Hosseini A, Li (December 2009). "Tibiofemoral and patellofemoral kinematics after reconstruction of an isolated posterior cruciate ligament injury: in vivo Analysis during lunge". Am J Sports Med **37** (12): 2377–85. Doi: 10.1177/0363546509341829. PMID 19726621
37) Boss AP, Hintermann B. Anatomical study of the medial ankle ligament complex. Foot Ankle Int. 2002; 23: 547–553.
38) Milner CE, Soames RW. Anatomy of the collateral ligaments of the human ankle joint. Foot Ankle Int. 1998; 19: 757–760.
39) Pankovich AM Shivaram MS. Anatomical basis of variability in injuries of the medial malleolus and the deltoid ligament. I. Anatomical studies. Acta Orthop Scand. 1979; 50: 217–223.
40) Sarrafian SK. Anatomy of the foot and ankle. Descriptive, topographic, functional. 2. Philadelphia: Lippincott; 1993. pp. 159–217.
41) Boruta PM, Bishop JO, Braly WG, et al. Acute ankle ligament injuries; a literature review. Foot Ankle. 1990; 11: 107–113.
42) Bekerom MPJ, Oostra RJ, Golanó P, et al. The anatomy in relation to injury of the lateral collateral ligaments of the ankle: a current concepts review. Clin Anat. 2008; 21: 619–626. doi: 10.1002/ca.20703.
43) Milner CE, Soames RW. Anatomical variations of the anterior talofibular ligament of the human ankle joint. J Anat. 1997; 191: 457–458. doi: 10.1046/j.1469-7580.1997.19130457.x.
44) Agur, Anne M.; Ng-Thow-Hing, Victor; Ball, Kevin A.; Fiume, Eugene; McKee, Nanacy Hunt (2003). "Documentation and Three-Dimensional Modelling of Human Soleus Muscle Architecture". Clinical Anatomy **16** (4): 285–293. doi:10.1002/ca.10112. PMID 12794910
45) Hodgson, JA; Finni, T; Lai, AM; Edgerton, VR; Sinha, S (May 2006). "Influence of structure on the tissue dynamics of the human soleus muscle observed in MRI studies during isometric contractions". J Morphol **5** (267): 584–601. Doi:10.1002/jmor.10421. PMID 16453292
46) Botta G, Piccinetti A, Giontella M, Mancini S (2001). "Il potenziamento dell'attività di pompa venosa del tricipite surale in ortopedia e traumatologia mediante l'utilizzo di una nuova apparecchiatura di ginnastica vascolare" [Strengthening of venous pump activity of the sural tricipital in orthopaedics and traumatology by means of a new equipment for vascular exercise] (PDF). Giornale Italiano di Ortopedia e Traumatologia (in Italian) **27**: 84–8.

47) Ariano MA, Armstrong RB, Edgerton VR (January 1973). "Hindlimb muscle fiber populations of five mammals". The Journal of Histochemistry and Cytochemistry **21** (1): 51 doi: 10.1177/21.1.51. PMID 4348494.
48) Burke RE, Levine DN, Salcman M, Tsairis P (May 1974). "Motor units in cat soleus muscle: physiological, histochemical and morphological characteristics". The Journal of Physiology **238** (3): 503–14. PMC 1330899. PMID 4277582
49) Clinically Oriented Anatomy. pp. 598–600. ISBN 978-1-60547-652-0.
50) Hamilton, Nancy; Luttgens, Kathryn (2001). Kinesiology: Scientific Basis of Human Motion (10th Ed.). McGraw-Hill. ISBN 978-0-07-248910-1.

APPENDIX A

The number of stress cycles of the knee joint can be calculated where the velocity of the synovial fluid lies in the following range:

STRESS	SHEAR RATE	$F(v_2) - F(v_1)$	No. of cycles
1211	157.88	$2.333288*10^{-4}$	$4.7828*10^{4}$
1420	173.76	$2.3329*10^{-4}$	$4.7820*10^{4}$
1650	189.64	$2.33253*10^{-4}$	$4.7813*10^{4}$
1905	205.52	$2.33217*10^{-4}$	$4.7805*10^{4}$
2188	221.4	$2.33179*10^{-4}$	$4.7797*10^{4}$
2501	237.28	$2.33142*10^{-4}$	$4.7790*10^{4}$
2846	253.16	$2.33106*10^{-4}$	$4.7783*10^{4}$
3221	269.04	$2.33069*10^{-4}$	$4.7775*10^{4}$
3630	285	$2.33032*10^{-4}$	$4.7767*10^{4}$

Table 1.12 Calculated data of the load cycle (from 5.0071m/sec to 5.01425m/sec)

STRESS	SHEAR RATE	$F(v_2) - F(v_1)$	No. of cycles
112500	5000	$7.023857*10^{-3}$	$1.4398*10^{6}$
120000	5500	$6.99048*10^{-3}$	$1.4329*10^{6}$
130000	6000	$6.95744*10^{-3}$	$1.4261*10^{6}$
140000	6500	$6.9247*10^{-3}$	$1.4194*10^{6}$
155000	7000	$6.892266*10^{-3}$	$1.4128*10^{6}$
170000	7500	$6.860135*10^{-3}$	$1.4062*10^{6}$
175000	8000	$6.828303*10^{-3}$	$1.3996*10^{6}$
180000	8500	$6.796763*10^{-3}$	$1.3932*10^{6}$
200000	9000	$6.765516*10^{-3}$	$1.3868*10^{6}$

Table.1.13 Calculated data of the load cycle (from 5.225m/sec to 5.45m/sec)

STRESS	SHEAR RATE	$F(v2) - F(v1)$	No. of cycles
112500	5000	$8.681344*10^{-3}$	$1.368874*10^{6}$
120000	5500	$8.630424*10^{-3}$	$1.360845*10^{6}$
130000	6000	$8.580109*10^{-3}$	$1.352911*10^{6}$
140000	6500	$8.53037*10^{-3}$	$1.345068*10^{6}$
155000	7000	$8.481206*10^{-3}$	$1.337316*10^{6}$
170000	7500	$8.432605*10^{-3}$	$1.329653*10^{6}$
175000	8000	$8.384558*10^{-3}$	$1.322077*10^{6}$
180000	8500	$8.33705*10^{-3}$	$1.314586*10^{6}$
200000	9000	$8.290088*10^{-3}$	$1.307181*10^{6}$

Table.1.14 Calculated data of the load cycle (from 4.225m/sec to 4.45m/sec)

STRESS	SHEAR RATE	$F(v_2) - F(v_1)$	No. of cycles
488	95.6	$4.6216*10^{-5}$	$9.4735*10^{3}$
559	101.54	$4.6207*10^{-5}$	$9.4716*10^{3}$
626	107.32	$4.6197*10^{-5}$	$9.4696*10^{3}$
692	113.11	$4.6194*10^{-5}$	$9.4690*10^{3}$
757	118.88	$4.6176*10^{-5}$	$9.4653*10^{3}$
822	124.66	$4.6162*10^{-5}$	$9.4624*10^{3}$
887	130.44	$4.6152*10^{-5}$	$9.4604*10^{3}$
953	136.22	$4.6142*10^{-5}$	$9.4583*10^{3}$
1020	142	$4.6129*10^{-5}$	$9.4557*10^{3}$

Table.1.14 Calculated data of the load cycle (from 2.5045m/sec to 2.5071 mt/sec)

Stress	Shear Rate	$F_{(v_1)} - F_{(v_2)}$	No. Of cycles
1211	157.88	$1.26741*10^{-4}$	$2.5979*10^{4}$
1420	173.76	$1.26653*10^{-4}$	$2.5961*10^{4}$
1650	189.64	$1.26567*10^{-4}$	$2.5944*10^{4}$
1905	205.52	$1.26492*10^{-4}$	$2.5928*10^{4}$
2188	221.4	$1.26406*10^{-4}$	$2.5911*10^{4}$
2501	237.28	$1.26319*10^{-4}$	$2.5893*10^{4}$
2846	253.16	$1.26244*10^{-4}$	$2.5878*10^{4}$
3221	269.04	$1.26158*10^{-4}$	$2.5878*10^{4}$
3630	285	$1.26071*10^{-4}$	$2.5842*10^{4}$

Table.1.15 Calculated data of the load cycle (from 2.5071m/sec to 2.51425m/sec)